TOPICAL REVIEW

Review of Patch Antennas used in Drone Applications

M. M. HASAN MAHFUZ, (Graduate Student Member, IEEE), AND CHAN-WANG PARK, (Member, IEEE)

Department of Electrical Engineering, University of Quebec at Rimouski, Quebec, QC G5L 3A1, Canada

Corresponding author: M. M. Hasan Mahfuz (mahm0036@uqar.ca)

ABSTRACT Drones are a form of remote-controlled aircraft that can take to the air without the need for a human pilot. An increasing number of people are looking into using drones for a variety of tasks, including but not limited to operations in hazardous areas, environmental monitoring and sensing, aerial spreading of fertilizer and agricultural chemicals, disaster management and transporting goods from one location to another. Drones are receiving a lot of attention for these and other uses. A drone's position and navigation can only be controlled by the remote pilot via radio frequency (RF) transmission between the drone and the remote pilot. In order to facilitate two-way communications between the drone and its operator, it is necessary to keep a tight eye on the telemetry data and supplementary sensor data being sent and received by the drone in real time. Unmanned flying would not be conceivable without a flexible and dependable communication system. Due to the necessity of complete spatial coverage for drone communication, the antenna radiating in an isotropic pattern presents itself as a promising option for unmanned flying. Therefore, microstrip patch antenna is an excellent choice for drone applications.

INDEX TERMS Drone communication, antenna design, phased antenna array, patch array, reconfigurable antenna, UWB radar, smart antenna, parasitic patch, triangle array antenna, realized gain, swarm drones, ground station and compact array antenna.

I. INTRODUCTION

The sophisticated processes and remarkable capacities of drones are servicing a significant part of the business. The use of drones in civil applications has gained significant traction in recent years [1]. There are many different kinds of drones, but they may be divided into two broad categories: those that are used for reconnaissance and surveillance, and those are used in scientific research [2], [3], [4], [5]. Drones are currently being used in the following human endeavors: agricultural, aerial photography, search and rescue, shipping and delivery, 3D mapping, safety surveillance, wireless internet access, research, and natural science. Drones are no longer a cutting-edge novelty but a crucial component of 21st century [6]. Despite this, many variants have been released and sold commercially in recent years, and

their popularity among end users has grown substantially. Drones are remotely piloted aircraft that can be equipped with cameras for use in videography and photography [7], [8]. Drones will be indispensable for many future uses, such as the surveillance of infrastructure from above, such as in manufacturing facilities, farms and other agricultural areas, and emergency response operations [9], [10]. Drones can be classified into subsets based on physical characteristics like size and weight as well as performance metrics like maximum altitude reached and flying range [11]. Fixed-wing aircraft and multicopter aircraft are the two primary categories [12].

Drones capable of traversing long distances make use of a narrow bandwidth. Ionosphere reflections and low-attenuation windows in the atmosphere make long-distance communications possible [13]. As part of the transition from analogue to digital television in Japan, the Ministry of Internal Affairs and Communications (MIC) reallocated the 169 MHz band in 2016 for use by autonomous vehicles

The associate editor coordinating the review of this manuscript and approving it for publication was Mohammad Zia Ur Rahman.
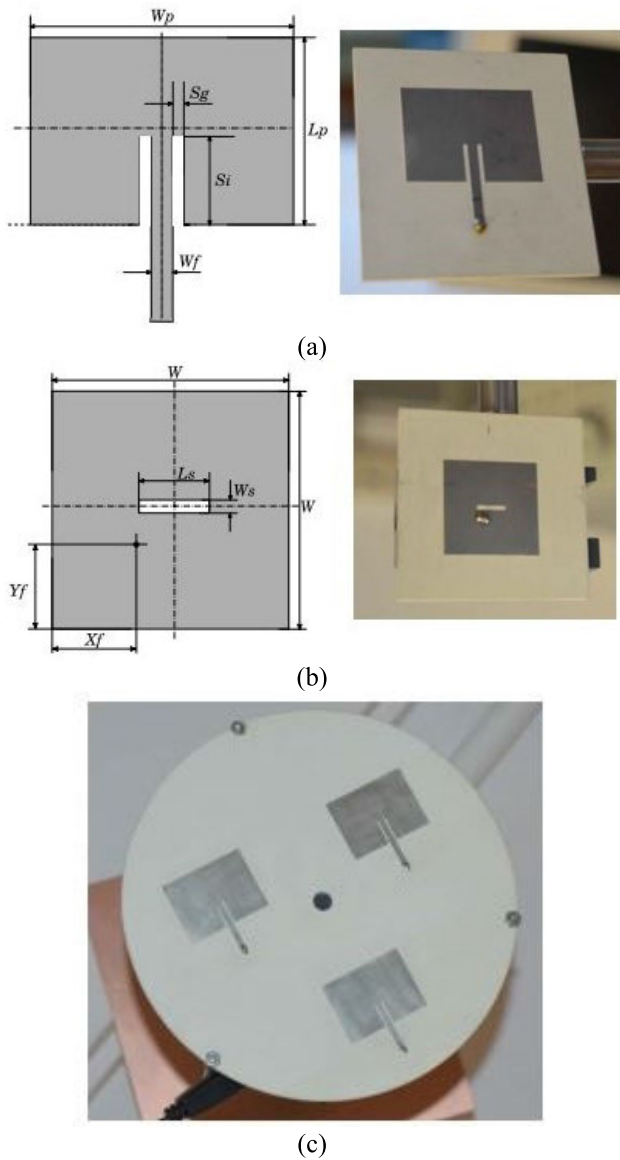
FIGURE 1. (a) Linear and (b) circular polarized antenna and (c) fabricated porotype [23].

FIGURE 2. S_{11} of proposed (a) circularly and (b) linearly polarized antenna [23].

including robots and drones. Drone operations across long distances and around barriers like buildings, trees, or terrains will benefit from this band's supposedly high range and favorable diffraction characteristics [14]. HF antennas are quite huge in comparison to the size of the drone because of their relatively modest dimensions. Low radiation resistance and intrinsic conductor losses are the two main drawbacks of this narrowband antenna design. As a result, small drones shouldn't use broadband antennas that work in the HF to lower-UHF bands [15]. Therefore, to reduce the antenna size, multiple antenna methods are created and applied for different frequency bands. The drone's materials and electronics must also be considered while constructing the antenna for placement on the drone's platform, as they may have an effect on the antenna's performance [16].
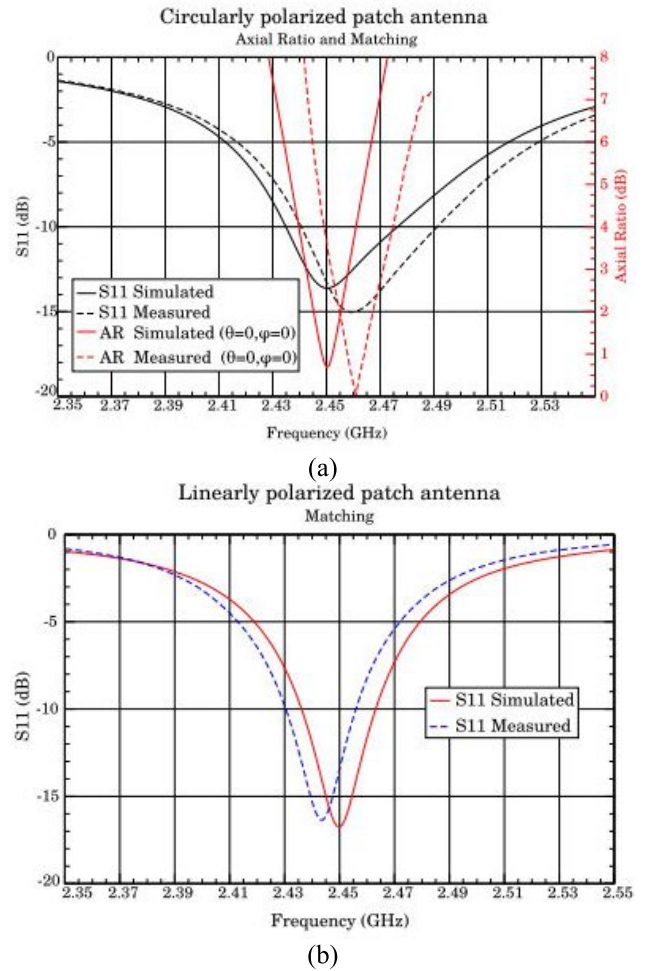
Microstrip antennas are rapidly improving in popularity and are now widely used in a variety of cutting-edge microwave systems [17], [18]. The rapid expansion of microstrip antenna applications and usage has stimulated ongoing research aimed at refining and enhancing the technology's fundamental properties. In most cases, the low gain of a microstrip antenna is traded off for a narrower frequency range. The microstrip antenna offers many benefits over the traditional microwave antenna, including its small size, low weight, conformability to substrate surfaces, low cost and ease of integration with other circuits [19]. The inventor of a microstrip antenna possibilities are presented in a comprehensive manner. The antenna design goal can be achieved by modifying the designer's selection of substrate type, antenna structure, perturbation type, and feeding method. In order to transfer massive amounts of data in real time, wireless drones communication systems require certain conditions to be meet [20]. Consequently, the drone's antenna system needs to be carefully developed [21], [22]. This survey paper presents the recent study of microstrip patch antennas used in drone communications.
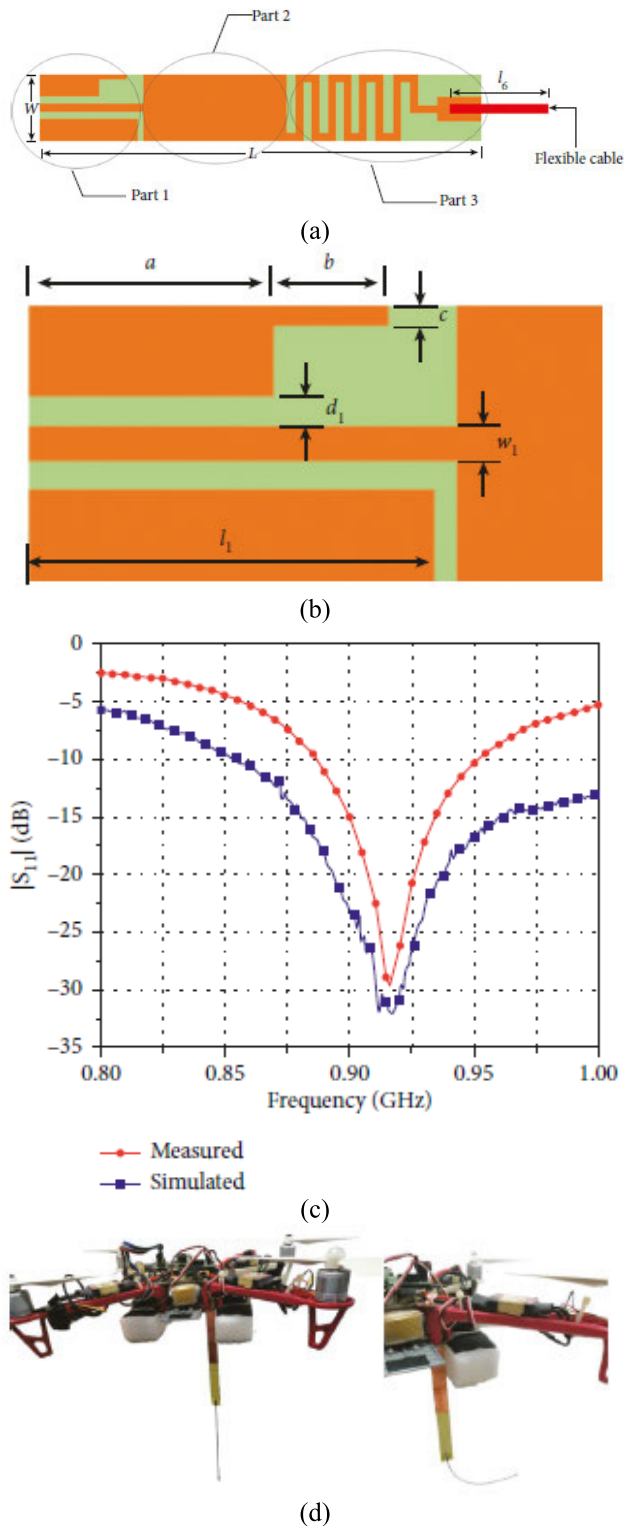
(a)

(b)

(c)

(d)

FIGURE 3. (a, b) Geometry of flexible UAV's antenna, (c) S_{11} & (d) antenna based drone display flexibility [24].

(a)

(b)

FIGURE 4. Comparison of simulated and measured 2–D radiation pattern, (a) E-Plane & (b) H-Plane [24].

II. PATCH ANTENNAS WITH SUBSTRATE
A. SINGLE BAND ANTENNAS

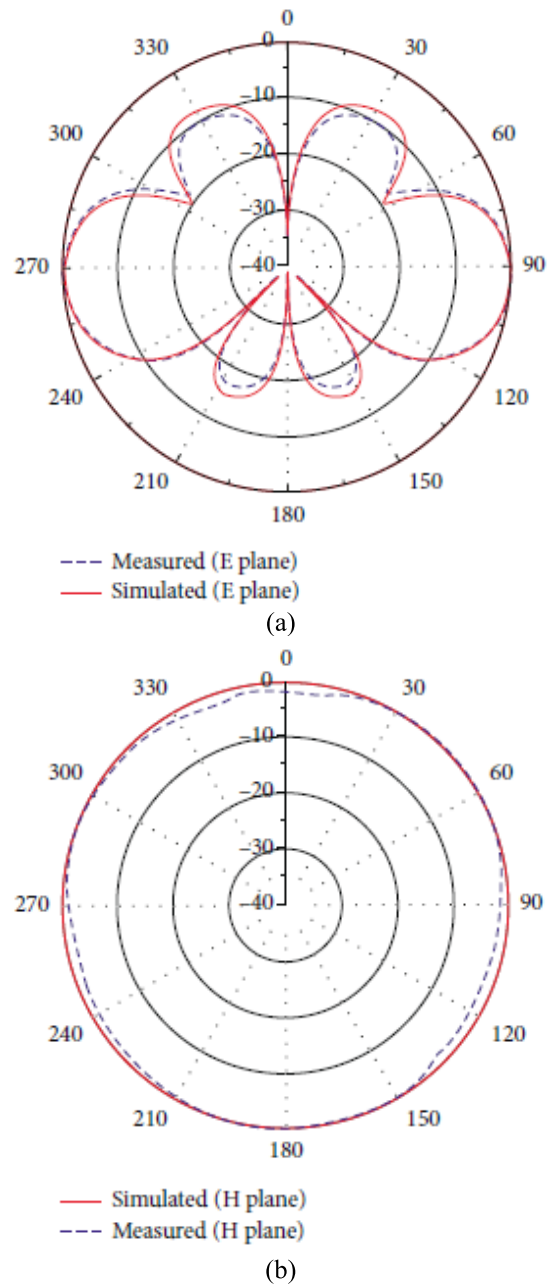Antennas are essential to every drone, quadcopter or unmanned aerial vehicle (UAV). Signal strength is the most essential element in the efficient operation of any drone whether it be for commercial, recreational or other purposes. It is impossible to imagine without computer simulation and optimizations, how different individual antennas are constructed for this purpose in order to attain the desire outcomes. Therefore, a squared microstrip patch (Fig. 1) that is coax-fed provide the circularly polarized antenna [23]. Circular polarization is achieved through the excitation of two orthogonal modes based on the slot size (W_S =1 mm, L_S =6.5 mm) and feed location (Xf=7.8 mm, Yf=7.8 mm). By changing the position of the feed along the patch diagonal,
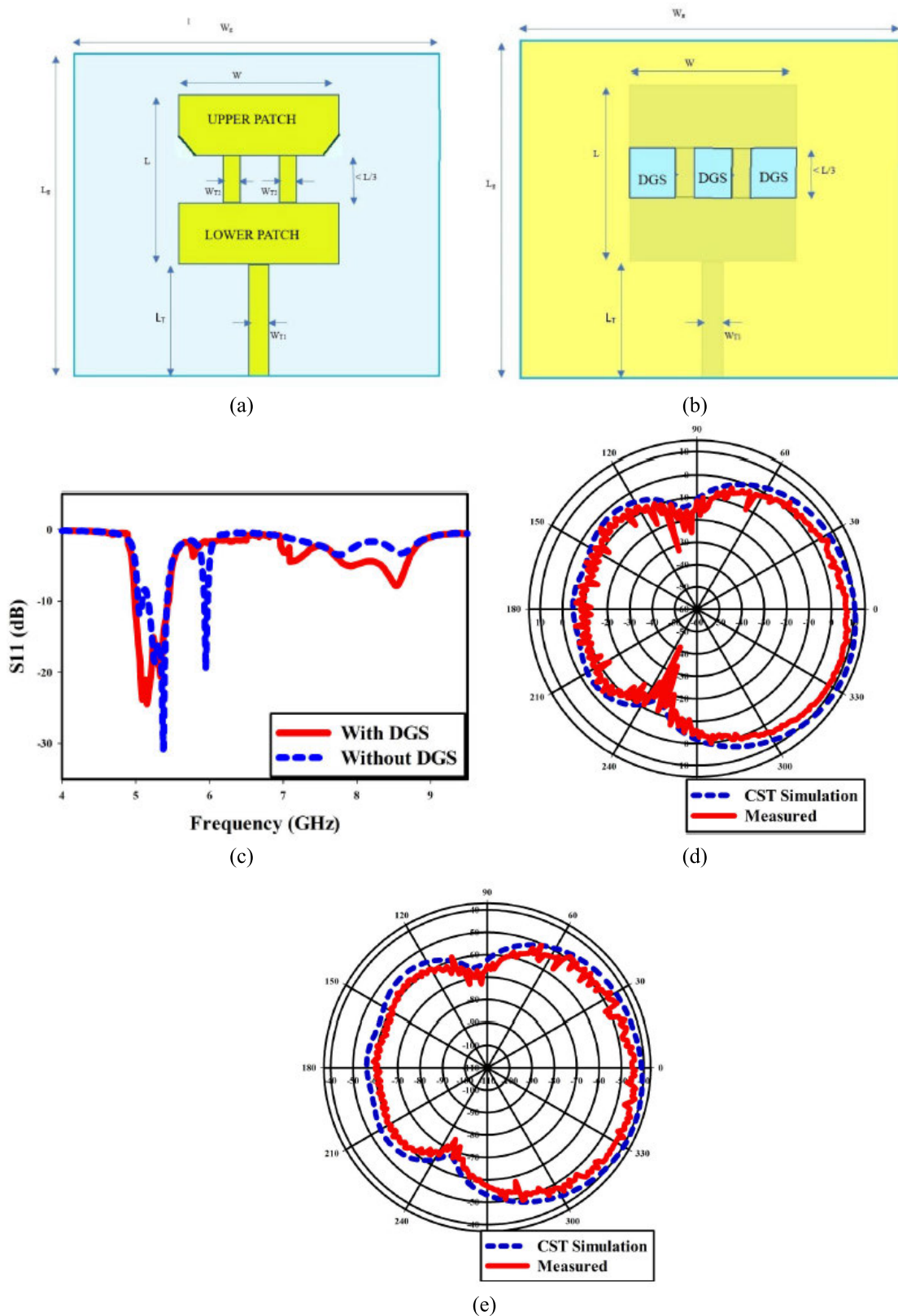
FIGURE 5. (a, b) Conformal patch antenna's top, bottom view, (c) S_{11} and (d, e) E & H-Plane [25].
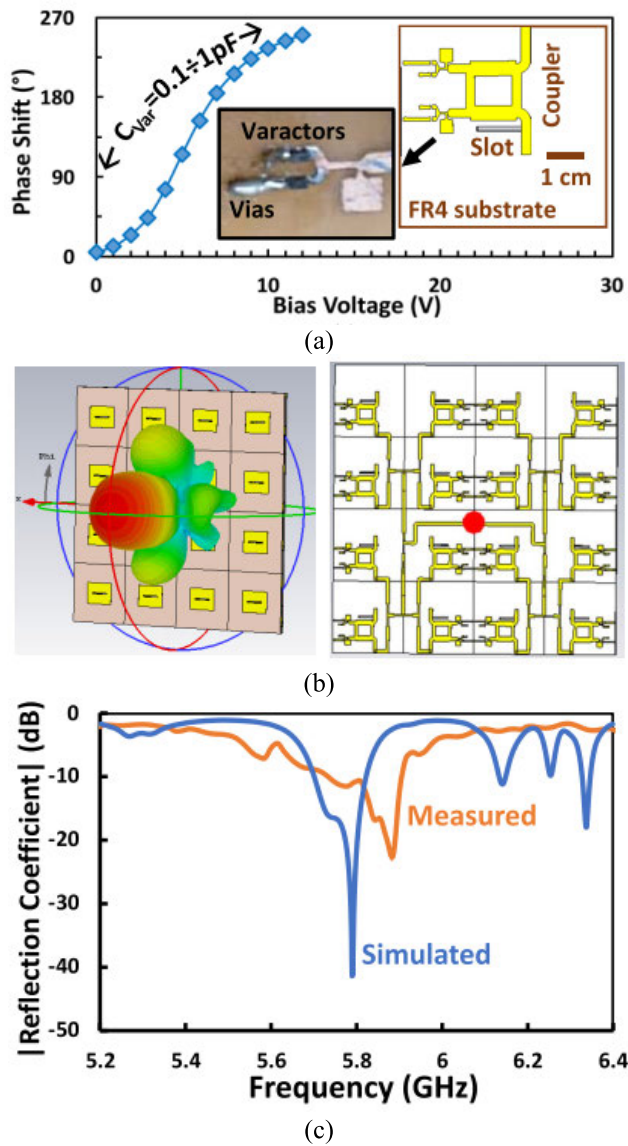
(a)

(b)

(c)

FIGURE 6. (a) Load capacitance as a parameter vs phase shift as a function of bias voltage, (b) design of a 4 × 4 phased array antenna and feeding network and (c) the phased antenna array's measured and simulated combined S_{11} at 5.8 GHz [26].

(a)

(b)

FIGURE 7. (a) 1 × 4 array antenna's top & bottom view, (b) overall arrangement of the proposed antenna [27].

the patch input impedance matching was optimized. Each antenna in the array is a rectangular microstrip patch with a feed inset (Fig. 1). The properties of the substrate and the resonance frequency (2.46 GHz) are used to calculate the patch's dimensions Wp=32.4 mm, Lp=24.2 mm. The antenna is fabricated on Rogers RO4360G2 substrates with dimension, D=7cm which is 1.524 mm in height with relative permittivity 6.15. Because of the substrate's high relative permittivity, the resulting patches are not excessively large. Altering the feedline slots' width (Si=9.2 mm) and length (Sg=0.6 mm) improves the patch's input impedance matching. S_{11} is depicted in Fig. 2 for both circularly and linearly polarized antennas. In addition, the axial ratio of a circularly polarized antenna is shown in Fig. 2 (a).
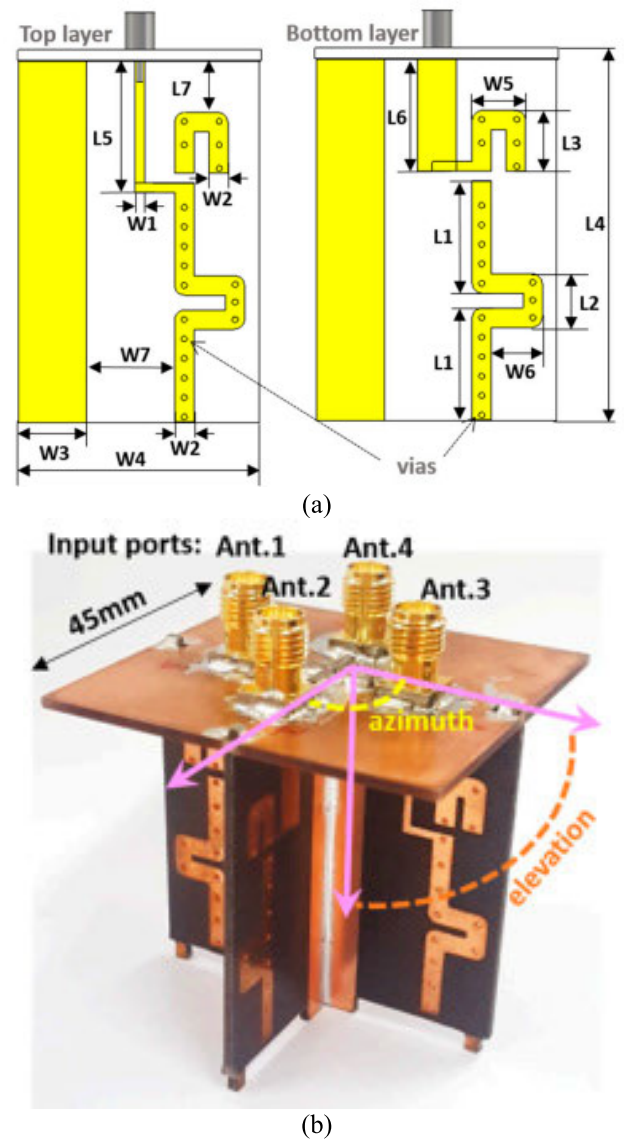
This research [24] presents a miniature, flexible, high-gain UAV antenna. The suggested antenna was essentially a series of three printed patches etched on a dielectric substrate. In addition, a flexible wire is anchored to the dielectric substrate, illustrated in Fig. 3 (a, b). To ensure proper impedance matching, a coplanar waveguide (CPW) with an asymmetric ground feeding structure is used. This pliable cable is made from stainless steel and has a 2 mm diameter. The UAV antenna's measured and simulated S_{11} over its (902–928) MHz bandwidth is shown in Fig. 3(c). To illustrate, Fig. 4 (a, b) depicts a linearly polarized all-encompassing radiation pattern. Though compact in size, the antenna's gain is impressively great. This demonstrates that the antenna's radiation pattern is nearly omnidirectional. This is because omnidirectional radiation in the horizontal plane allows the drone's antenna to cover signals from any direction.
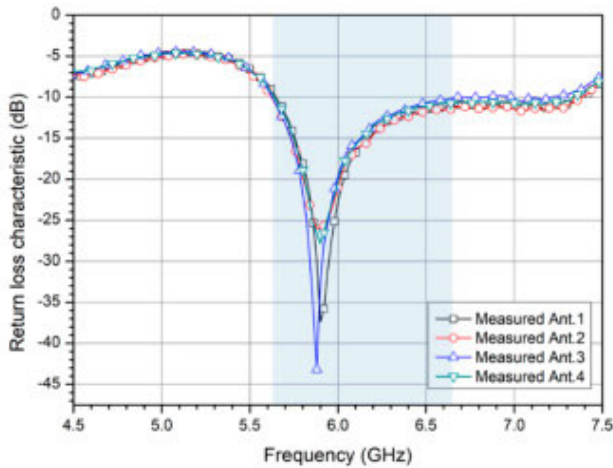
FIGURE 8. Measured S_{11} of the proposed 1 × 4 array antenna [27].

In particular, as seen in Fig. 1(d), the drone's flexible cable can be bent during landing and straightened out during take-off. Therefore, the radiated patch printed on the dielectric substrate is replaced with a flexible cable, and the antenna end is incorporated into the drone's design to reduce air resistance.

This research presents [25] a conformal patch antenna layout, which can be used in aircraft for tasks like monitoring water currents from above. The current system uses frequencies in the C-band (5.05–5.45) GHz because this is the optimal range taking into account the decorrelation time, precipitation, resolution, and antenna size. The improved cross-range resolution is a result of the 7.7% bandwidth attained in this design. The bore side angle is where a gain of 10 dB is attained. The effect of using a deflected ground structure (DGS) to dampen higher-order harmonics has been modelled and described. Two patches, a quarter-wave transformer, two microstrip lines joining the patches, a ground plane, and a ground plane with DGS slits carved into it make up this construction illustration in Fig. 5 (a, b). These two patches, which are roughly the same size, both resonate (5.2 GHz) at the intended frequency. Simulated and experimental placement of the antenna on CFC sheets reveals minimal effect. The entire bandwidth's (5.05–5.45) GHz return loss –10dB, it's illustrated in Fig. 5 (c). Results from an anechoic chamber measurement of the E-field and H-field are shown in Fig. 5 (d, e).

For its optimal compromise between loss, matching performance, and compactness, a reflection-type phase shifter architecture using a four-port branch line coupler and two reactive variable loads was chosen [26]. On a Rogers TM4 substrate (ε_r =4.5), a 35μm copper cladding method was used to build the 16 phase shifter unit cells. In order to adjust the reactive load, four ultra-small diode varactors were soldered together as shown in Fig. 6(a). Before being incorporated into the phased array, each phase shifter was

tested independently, which required the soldering of SMA connectors. The goal was to create a 4 × 4 element microstrip antenna array (Fig. 6b) with adequate gain, scanning resolution, and side lobe compression with minimal fabrication cost and encumbrance. The combination of measured and simulated of 4 × 4 phase array antenna's S_{11} shows in Fig. 6(c).

This work [27] proposed a highly effective antenna array with a tilted-beam characteristic and 360° of beam coverage for use in radar applications installed on unmanned aerial vehicles (UAVs). Four 2-dimensional ground reflectors are used to create four planar super J-pole antennas to form the suggested array antenna. A UAV's bottom super J-pole antenna element has a strong directivity, with the peak gain slanted at an angle of around 45° downward. This effectively resolves the problem of air-to-ground communication between the UAV and ground targets caused by the difference in altitude between the two. In addition, the four super J-pole components may cover a 360° arc around the UAV with switched operation while keeping a very high antenna gain. The top and bottom conducting layers of the single super J-pole antenna element are shown in Fig. 7(a); these layers are joined to one another vias to produce an electrically thick conductor. A complete configuration of the suggested antenna array, using four identical super J-pole antennas with 2-dimensional reflectors, is shown in Fig. 7(a). The suggested antenna structure is compared to a standard J-pole antenna by creating three types of planar J-pole antennas at 5.9 GHz (Fig. 8) on a Taconic TLX-9 substrate with a relative permittivity of 2.5 and a thickness of 1.1 mm. The four antenna elements have HPBWs better than 60° and 87° measured in the azimuth plane illustrated in Fig 9. The minimum antenna gain of around 4 dBi was measured at the overlapped area in between the antenna elements, so even though the measured HPBW in the azimuth plane was smaller than the simulated result, the entire 360° coverage could still be provided with relatively high gain.

An UWB conformal antenna [28] with a revolutionary design that was presented for use in Unmanned Aerial Vehicle (UAV) applications. A 50Ω SMA connector is used to link the Y-round shaped patch element to a matching feed line, which supplies current to the complete conformal antenna illustrated in Fig. 10(a). Wider bandwidth is provided by the Y-rounded shape and the circular parasitic element. In order to fit on the wings of the quadcopter drone, this design proposes a low-profile antenna shown in Fig. 10 (b). Fig. 11 compares the measured and simulated S_{11} parameter with the antenna detached and attached to the UAV construction. The measured antenna was confirmed to perform flawlessly in the (2.9–15.9) GHz frequency range. For the frequency range of (3.1–6.0) GHz, the XZ-plane (φ =0°) displays the 2-D patterns in terms of the elevation angle for the main radiation cuts in Fig. 12. Variations in the patterns are tolerable. However, this proves the antenna's superior performance.
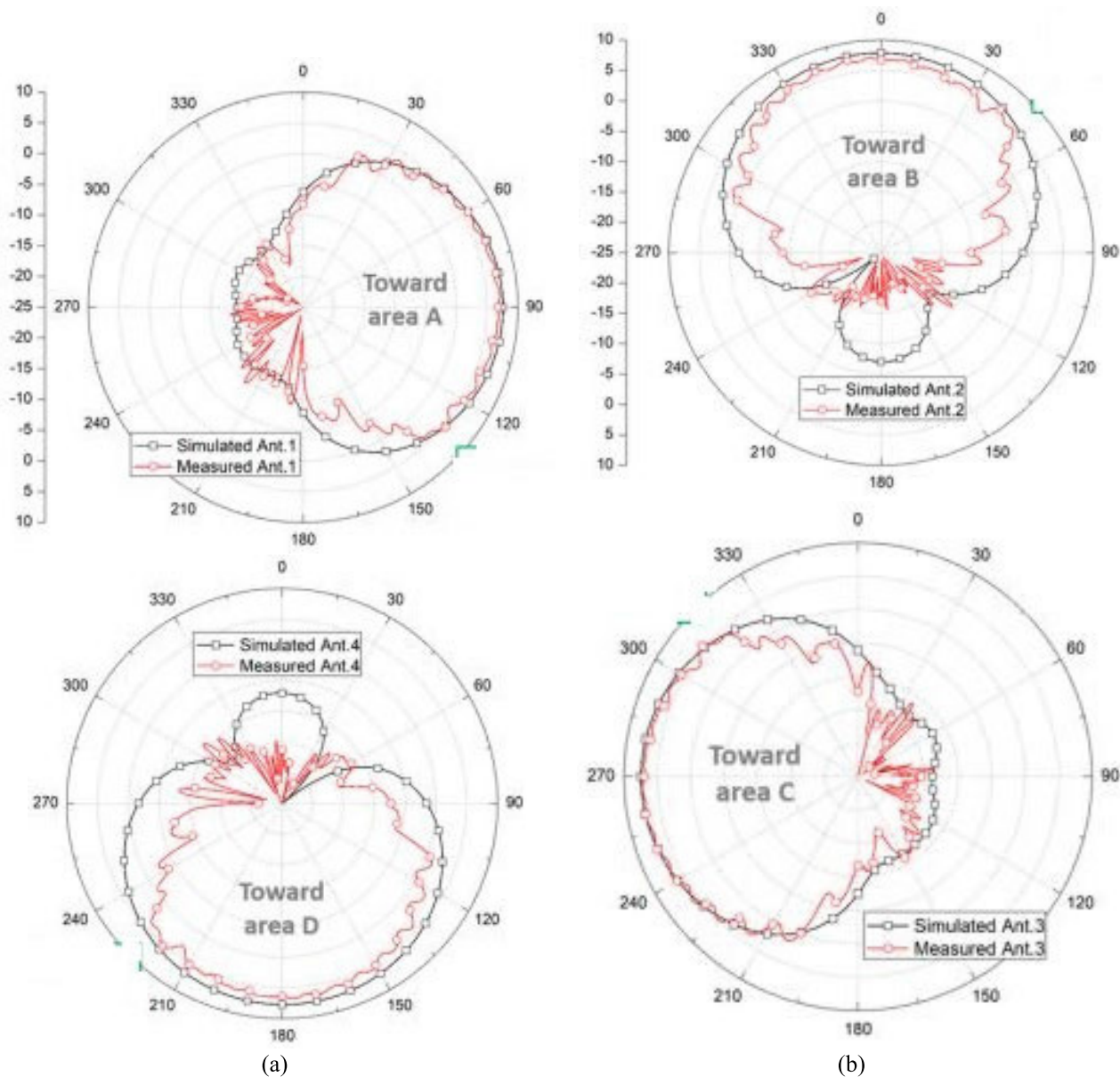
(a)   (b)

FIGURE 9. Measured 2-D radiation pattern at 5.9 GHz for azimuth plane [25].

Because the limited area for the antenna in the UAV is cylindrical in shape, this research [29] proposes two antenna designs for an UAV. The antennas are designed to work inside the 2.45 GHz Wi-Fi spectrum. The intended antennas consist of a circular array of four elements, each of which is a perfect cylinder. The fundamental radiating elements of both arrays are either a rectangular microstrip patch antenna or a PIFA antenna and illustrated in Fig. 13 (a, b). Both antenna arrays are shown to have good matching at the working frequency, and their simulated radiation patterns display a remarkably omnidirectional nature. The simulated return loss (S_{11}) and 2-D,3-D radiation pattern shows in Fig. 13 (c, d) respectively.

In order to improve drone communications, a planar antenna with a quasi-isotropic emission pattern is proposed [30]. The proposed antenna utilizes top loaded monopole antennas in conjunction with slotted loop antennas. To begin, a top-loaded 4-element monopole antenna is created to radiate in a monopole-like pattern. Fig. 14 depicts the proposed quasi-isotropic antenna's fabricated prototype. There are three elements making up the top-loaded monopole antenna. Both the top and bottom layers have a dielectric constant and loss tangent of 0.05, and they are both produced on a glass-reinforced epoxy laminate (FR4) substrate. Both the upper and lower layers are 0.6 mm thick (h1) and 1.6 mm thick (h2). The top ground plane, the top circular
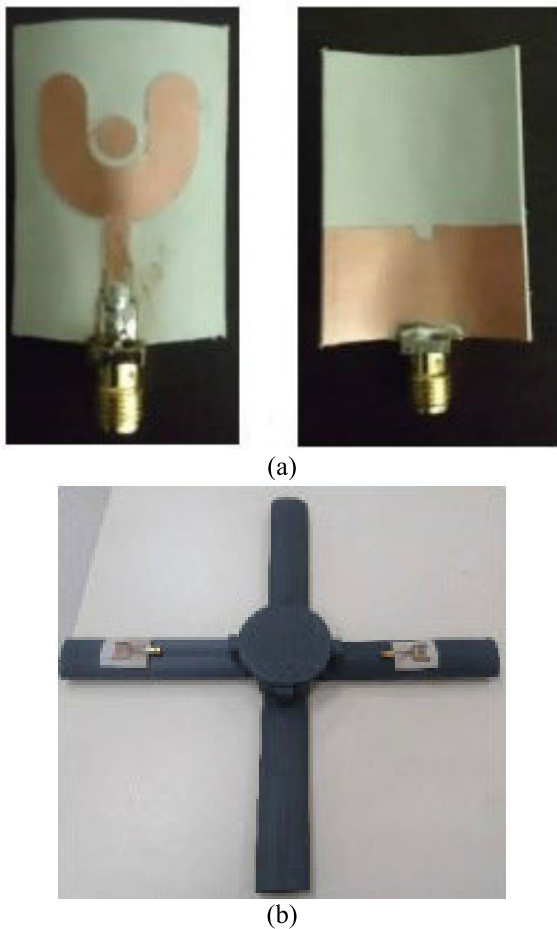
(a)

(b)

FIGURE 10. Fabricated conformal UWB antenna's (a) top & bottom view, (b) proposed antenna on UAV [28].

FIGURE 11. Proposed conformal UWB antenna's measured and simulated S$_{11}$ [28].

patch, and the feeding network together make up this layer. An Anritsu vector network analyzer is used to calculate the reflection coefficient of the proposed antenna. Good agreement between simulated and measured reflection coefficients is seen in Fig. 14 (c). The antenna's 3D radiation pattern, as measured, is displayed in Fig. 14 (d). No nulls were found in the measured 3-D radiation pattern, indicating that the antenna can cover full spatial coverage and is therefore classified as a quasi-isotropic antenna. The maximum gain of the antenna is 2.74 dBi, and the minimum gain is −10.22 dBi, for a total 3D volume gain deviation of 12.9 dBi.

In this study [31], introduced an unique 2.4 GHz virtual array for use in wireless connectivity in FANETs. The proposed architecture considers a random three-dimensional topology among eight nodes in a FANET. The most notable changes are that each node is now a rectangular patch antenna attached to a physically plausible aero plane frame. The optimal placement of nodes mitigates interference from aero plane parts. The FR4 substrate antenna is small and lightweight enough to be integrated into the drone's body. A simple rectangular patch antenna (Fig. 15a) with inset feeding method provides 2.4 GHz operating frequency. The patch
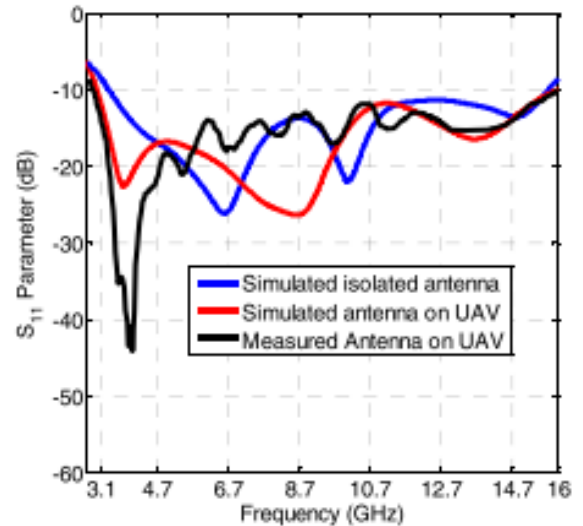
antenna was installed on a simulated drone during the testing phase and illustrated in Fig. 15(b). The S$_{11}$ characteristics of the drone-mounted patch antennas are shown in Fig. 15(c).

This paper, [32] proposed a small antenna for aircraft identification based on the demodulation of ADS-B communications; the antenna consists of an array of four PIFA antennas mounted above an RP (reflector plane) illustrated in Fig. 16 (a, b). This antenna comprises of an array of Planar Inverted-F Antennas, a quadrature feed network (FN) and a reflector plane and it is intended to be installed on the top of a drone in order to detect and avoid collisions with airliners. Patch and quasi-omnidirectional antennas are typically used in conjunction with one another for the purpose of detecting ADS-B signals. For the same purpose, a small T-Slot patch antenna is introduced and reasoned that a quasi-omnidirectional, circularly polarized antenna would be best for locating the distant aircraft. Good matching is evidenced by a value of less than −15 dB at 1.09 GHz, as plotted for the reflection coefficient as a function of frequency in Fig. 16(e). From this Figure depicted that, the orientated across the OZ-axis, which is perpendicular to the antenna plane, the antenna array with quadrature feed can reach its maximum gain of +4.85 dBi. The finalized feeding network design is depicted in Fig. 16(c). It is made up of several transmission lines joined together at a T-junction, each with its own unique characteristic impedance and length. An impedance transformer and a phase shifter of 90° respectively. Microstrip meander lines were also utilized for compactness in order to adhere to the designated for specific application i.e. 1.09 GHz. To achieve the desired phase shift between each antenna port, the length of the 50Ω line was modified to $\lambda/4$ as shown in Fig. 16 (c). The maximum gain of +4 dBi was achieved at 1.09 GHz with an elevation angle of 60° or in angular terms with $\theta = 30°$ as shown in Fig. 16 (f).
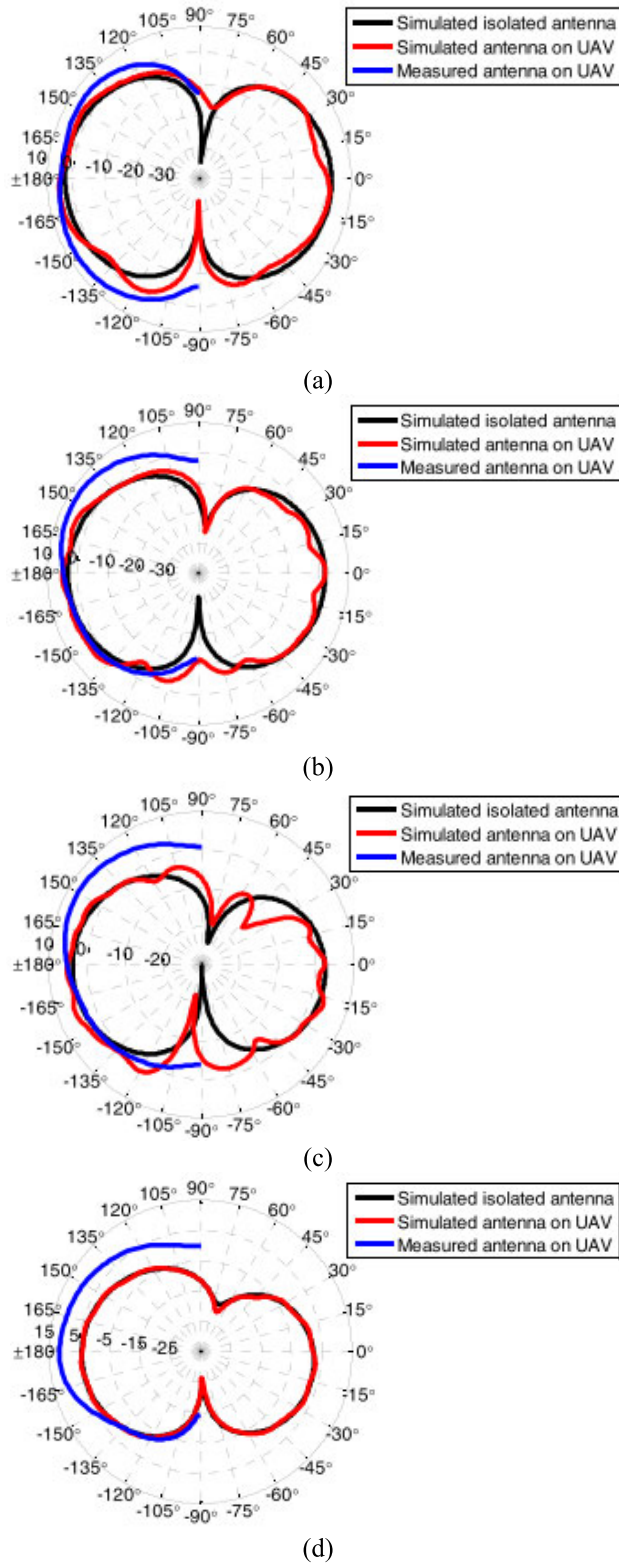
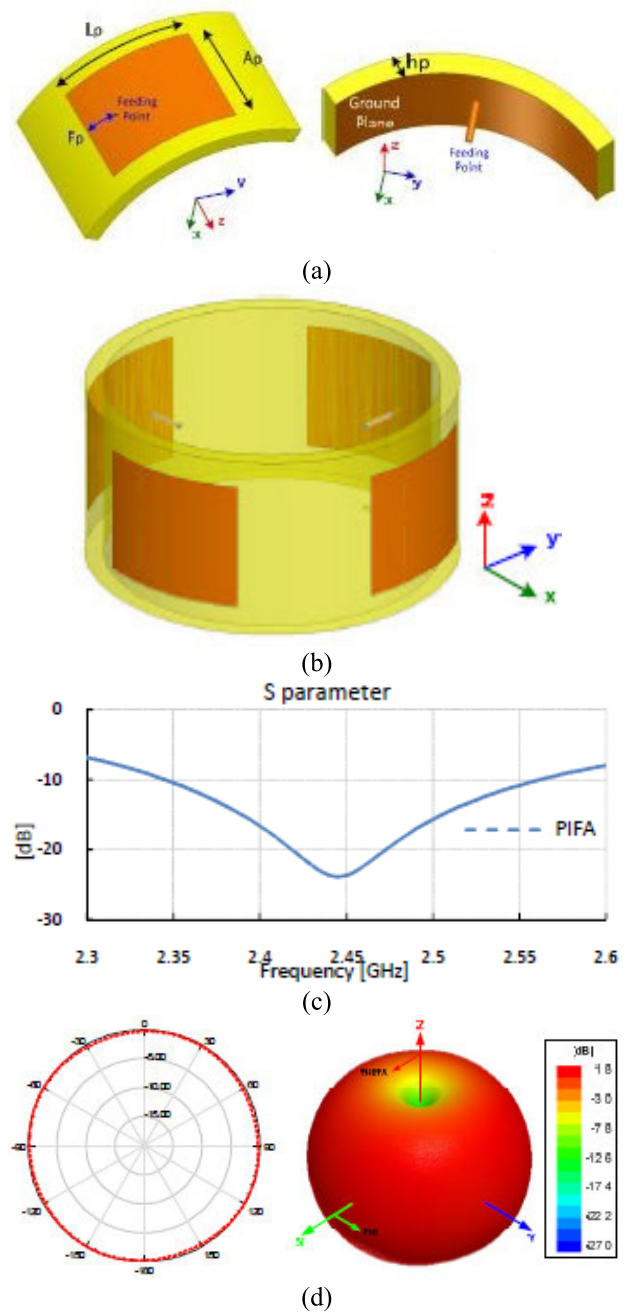FIGURE 12. 2-D radiation pattern of XZ-Plane at (a) 3.1 GHz, (b) 4.1 GHz, (c) 5.1 GHz and (d) 6 GHz [28].

FIGURE 13. Array element geometry (a) top and bottom perspectives, (b) Exhaustive array of rectangular patches, (c) simulated S_{11} and (d) XY-Plane with 3-D gain of the simulated radiation pattern for the PIFA array [29].

This paper presents a conical-beam high-gain planar antenna for use in millimeter-wave drones [33]. The

antenna design calls for a vertical monopole with circular side reflectors. The in-phase reflections from the planar annular-distributed side reflectors, which are accomplished by a series of via walls utilizing the printed-circuit-board (PCB) construction, result in the high-gain conical beam. The proposed construction, which is made up of two pieces of a via-based monopole antenna and a number of annular-distributed vias, is shown in an exploded view in Fig. 17(a). The monopole based on the vias behaves like a standard
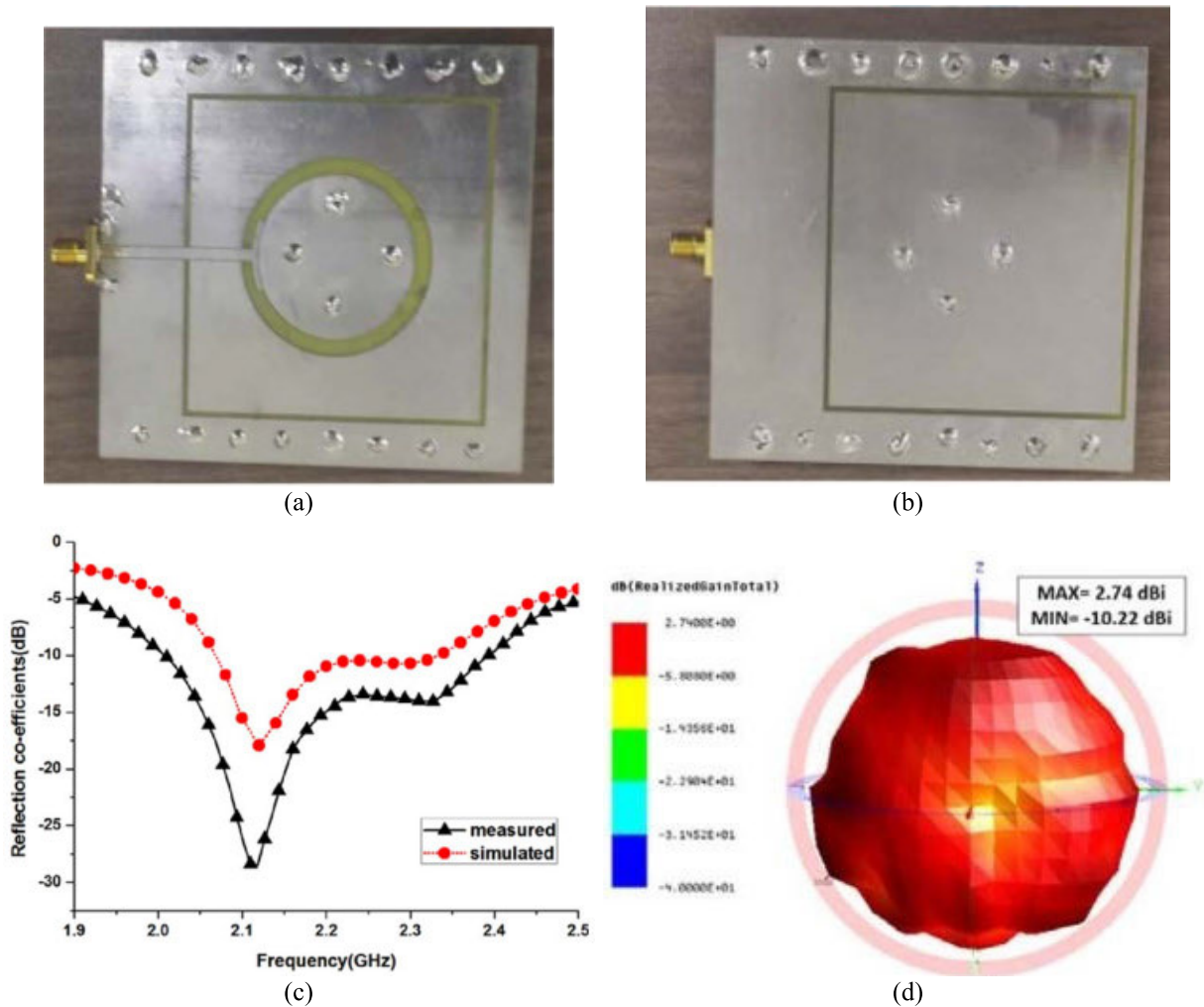
FIGURE 14. Fabricated proposed planar quasi isotropic antenna's (a) front, (b) bottom view, (c) S_{11} and (d) measured 3-D radiation pattern at 2.1 GHz [30].

quarter-wavelength monopole to produce radiation in all directions, while the annularly distributed vias are meant to act as side reflectors to focus the radiation on the desired beam direction beam pointing angle (BPA). Above a wide electrically conductive plane, the entire structure is probed for its electrical properties. An initial layer through a hole with a diameter of 0.6 mm (d1) is used to realize a source monopole in the proposed architecture. When using the PCB fabrication process, a little copper disc with a diameter of (d2) is placed on the top surface of the board to ensure the via hole is large enough. A copper ground plane, shaped like a circle, is used on the underside of this layer to build a monopole, but it must be kept at a safe distance from the monopole's through hole. For this reason, the proposed design features a non-copper area in the center of the ground plane with a diameter (d3) larger than the diameter of the monopole (d1). The via-based monopole is somewhat shorter than the length of the original monopole because of the two copper layers on both sides of the first substrate. The ground plane size

(b) has a significant impact, while the other three dimensions (d1, d2 and d3) have little or no influence. Good agreement is seen between the simulated and observed data, with a simulated –10 dB impedance BW of (26.50–29.96) GHz and a measured one of (26.63–29.91) GHz, illustrated in Fig. 17(b). When comparing the simulated and measured values, the fractional BW is 12.26 and 11.6%, respectively. Tolerances introduced by the assembly procedures account for the observable, albeit little difference. Two-dimensional radiation patterns at 27, 27.5, 28, and 28.5 GHz on the planes of $\varphi = 0°$ and $\varphi = 30°$ are shown for the suggested antenna in Fig. 18. At $\theta = 22°$, the maximal gain is 8.51 dBi, while at $\theta = 0°$, there is no radiation at all. Conical pattern at (27–28.5) GHz exhibits stable performance with little fluctuation of 1.42 dB in the peak gain and keeping the beam pointing angle at $\theta = 22°$ throughout the tested frequency range. Accordingly, the proposed design emits radiation with an effective CB shape, notable for its high peak gain and low loss.
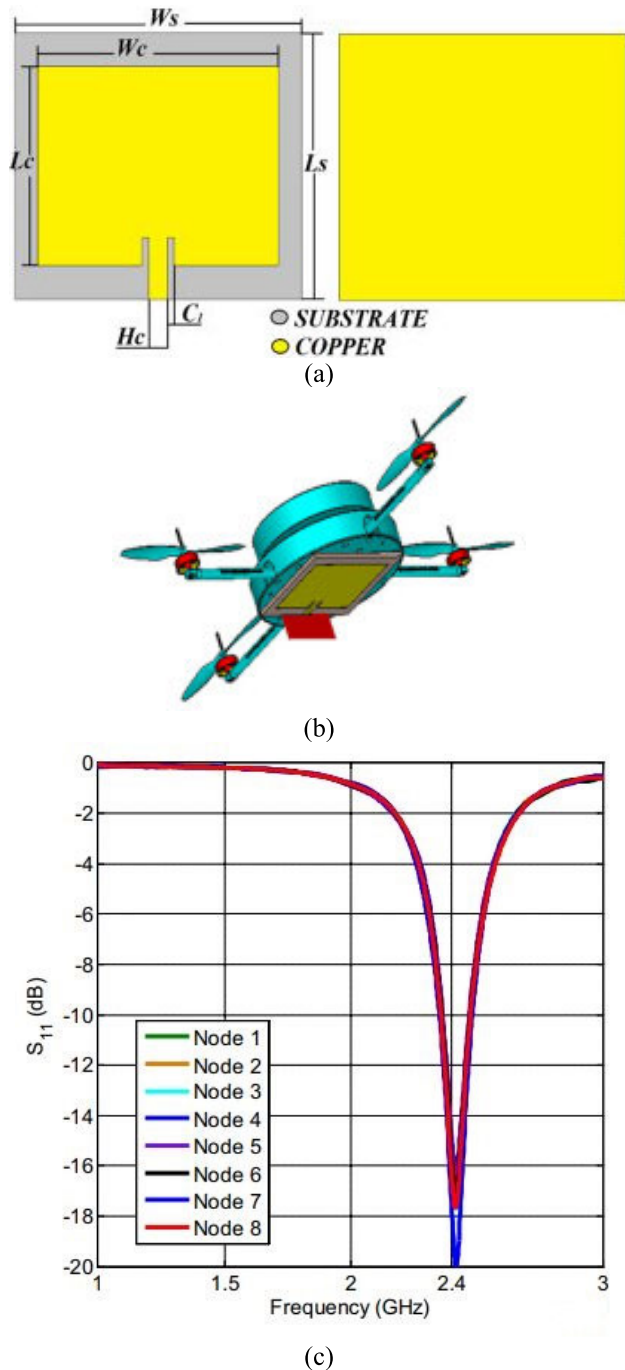
FIGURE 15. (a) Proposed rectangular shape antenna's top and back side view, (b) antenna placed on drone & (c) S$_{11}$ of this antenna [31].

In this study [34] suggested a compact Annular Ring (AR) microstrip antenna for UAVs. A standard annular ring antenna was built up to take advantage of an opportunity, and as a result, a working frequency of 2.4 GHz and a bandwidth of 160 MHz. The antenna is constructed using a metal cavity that is made up of two distinct substrates, as can be seen in Fig. 19(a). A circular conducting patch printed on an Isola IS680-280 substrate measures 0.8 mm in diameter, while a

standard FR-4 substrate serves as the lower layer. Using a single header pin, the top layer of the FR-4 substrate is connected to the circular patch antenna, while the bottom layer is connected to the cavity and serves as the reference ground plane. A microstrip line, with a characteristic impedance of 50Ω, is drawn in the top layer of the FR-4 substrate using the industry-standard 35μm copper thickness, and supplies feeding for the circular patch. Higher order modes were generated by connecting the circular patch with the FR-4 substrate using two additional headers, which increased the system's overall bandwidth. The AR antenna reflection coefficient is depicted in Fig. 19(b). The antenna has a total bandwidth of 160 MHz, covering a frequency range of (2.38–2.54) GHz (at a –10 dB reference level for parameter S$_{11}$). Fig. 19 (c) displays the results of a comparison between the co-polar and cross-polar components in the E- and H-planes.

In this work [15], suggested a strategy for developing a compact antenna system well suited for integration with multi-rotor drones. A flat radial power divider, as opposed to a Wilkinson power divider, is used to feed antennas attached to the propellers, as each of the several rotors is part of a branch connecting to the center of the drone. The quadcopter's wireless connection to the ground is design using at 2.4 GHz 4-way radial power divider and four antennas tuned to that frequency. The porotype illustrated in Fig. 20 (a) and simulated return loss (S$_{11}$) in Fig. 20 (b). All the curves in the PCB radial power-divider overlap, and the return loss is good at 2.4 GHz, thus it satisfies the criteria on equal-power division. The antenna array generates a far-field pattern that permits isotropic radiation in all directions shown in Fig. 20 (c). Moreover, the gain is 4 dBi, so the drone can communicate with the ground and other drones from a distance.

B. DUAL BAND ANTENNAS

The first proposed antenna design consists of a dual-band combo antenna made up of two optimized single-antenna designs, a rectangular patch antenna and a truncated patch antenna attached back-to-back, one facing the other [35]. Both single antennas are connected with the front and the rear side of the double-sided antenna, with the ground in the center of the configuration. This creates a double-sided antenna. The dimensions of the substrate and the ground of the antenna are the same, hence the rectangular patch's dimensions must be optimized for frequency and miniaturization. Two ports, one for the front side and the other for the back of the antenna, are included in the design. Both separate ports were used, and the front side antenna ran at 1.575 GHz while the back side antenna operated at 2.45 GHz. The dual band combo antenna's physical dimensions illustrated in Fig. 21. The S$_{11}$ for 1.575 GHz & 2.45 GHz truncated patch antenna is shown in Fig. 22 (a, b).

It is given a circular microstrip patch antenna operating on two frequencies (2.4 GHz and 5.2 GHz) for use in aircraft [36]. The envisioned antenna is fabricated on a Rogers
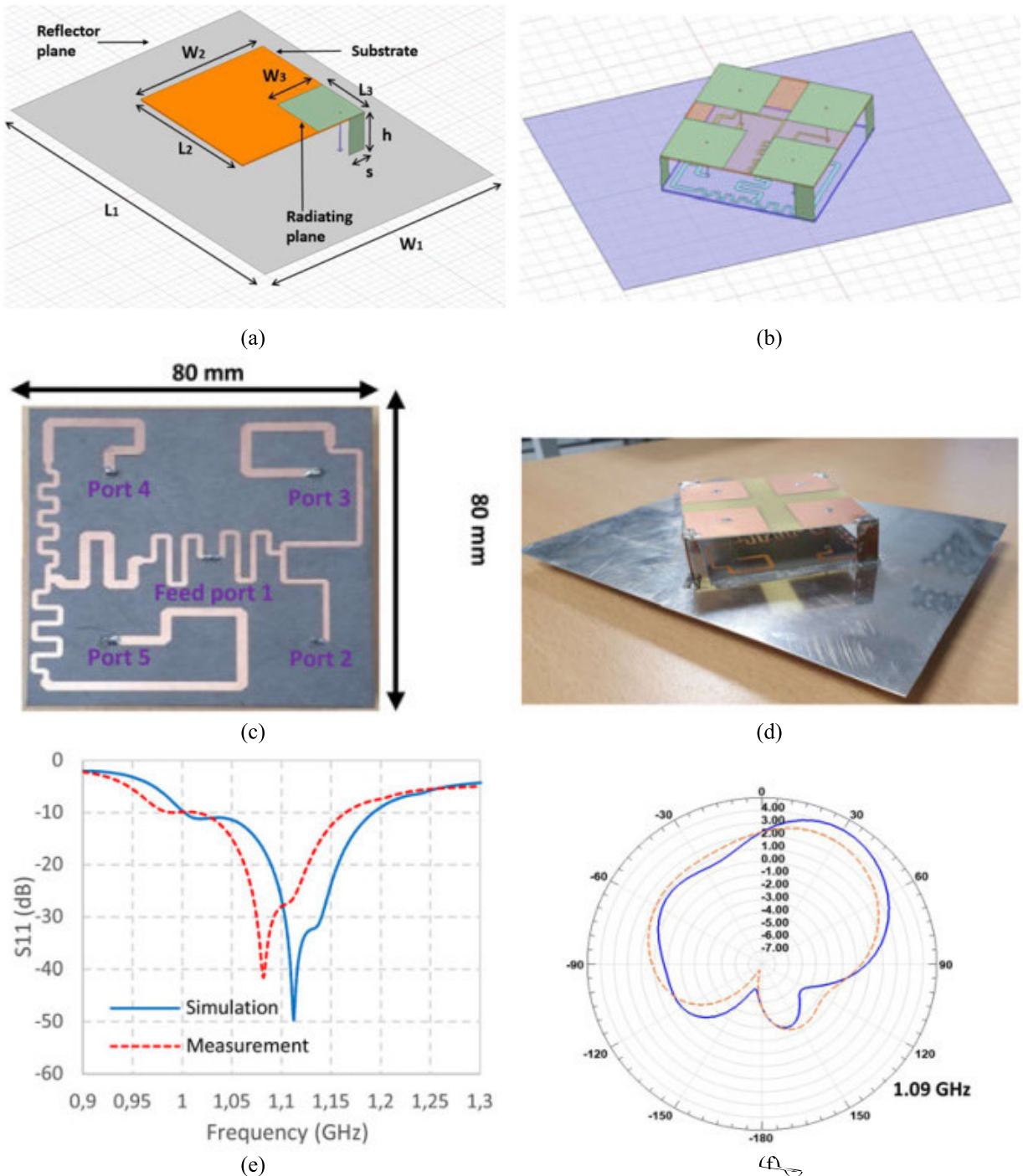
FIGURE 16. (a) Physical geometry of the antenna with single PIFA, (b) PIFA antenna array bottom and in isometric perspective, (c, d) fabrication of quadrature feed network, array antenna, (e) simulated S_{11} and (f) 2-D radiation pattern at 1.09 GHz [32].

5880 substrate ($\varepsilon_r = 2.2$ and $\tan\delta = 0.0009$), as displayed in Fig. 23. Each band's BW augmentation of the proposed antenna is carried out independently and displayed in Fig. 24. The driven patch is surrounded by parasitic patches or dummy patches that are used in the proximity parasite patch technique. Both the radiating edges and the non-radiating edges of the driven patch relate to the parasitic patches to it.

Fig. 25 (a, b) displays the measured far-field radiation patterns for the 2.4 and 5.2 GHz bands at the corresponding resonance frequencies. Gain measurements show a peak of 9.55 dBi at 2.4 GHz and 8.5 dBi at 5.2 GHz. The suggested antenna operates in the 2.4 GHz band with a dominant mode resonance (TM_{11}) and a broadside radiation pattern, and in the 5.2 GHz band with a higher-order mode resonance (TM_{01})
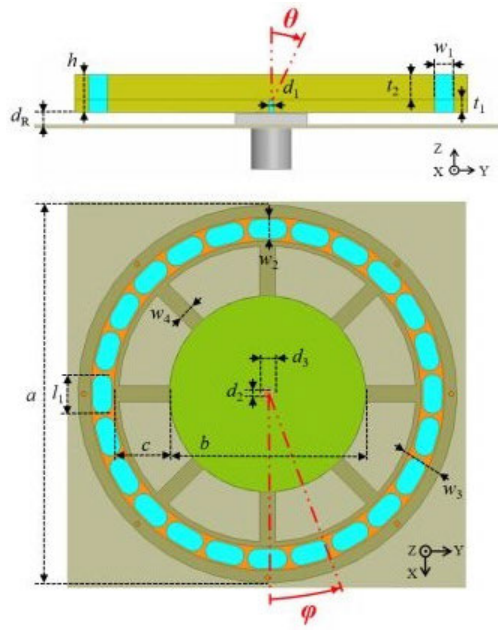
(a)
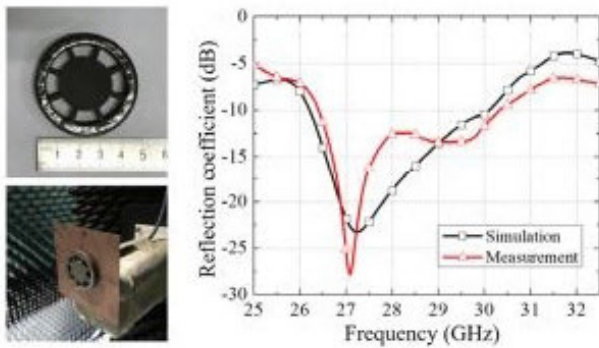
(b)

FIGURE 17. Specifics about the proposed antenna's shape: (a) side, top perspectives and (b) fabricated antenna & combination of measured, simulated S_{11} [33].

(a)

(b)

(c)

(d)

FIGURE 18. Combination of simulated & measured 2-D radiation pattern at (a) 27 GHz, (b) 27.5 GHz, (c) 28 GHz and (d) 28.5 GHz [33].

and a quasi-omnidirectional radiation pattern. With its high gain and respectable azimuth coverage, the suggested antenna has the potential to be an invaluable tool for unmanned aerial vehicles. This antenna's broader bandwidths at both the bands and its thin, flexible substrate make it superior to traditional monopole antennas in terms of data rate handling and practicality for HD video transmission over greater distances. Furthermore, this antenna might be mounted on a wing or fuselage of the UAV without compromising the vehicle's aerodynamics, which could improve its stability. By making small adjustments to the dummy patch radius, it is possible to set off several resonances. Minor shifts in the dummy patch radius might trigger several resonances. The gaps between the patches, which regulate how the antenna's impedance is matched, can be used to tune the coupling between them. At the feeding point, a SMA jack is linked to a plated via with a diameter of 1.2 mm. Conductive epoxy is used to connect
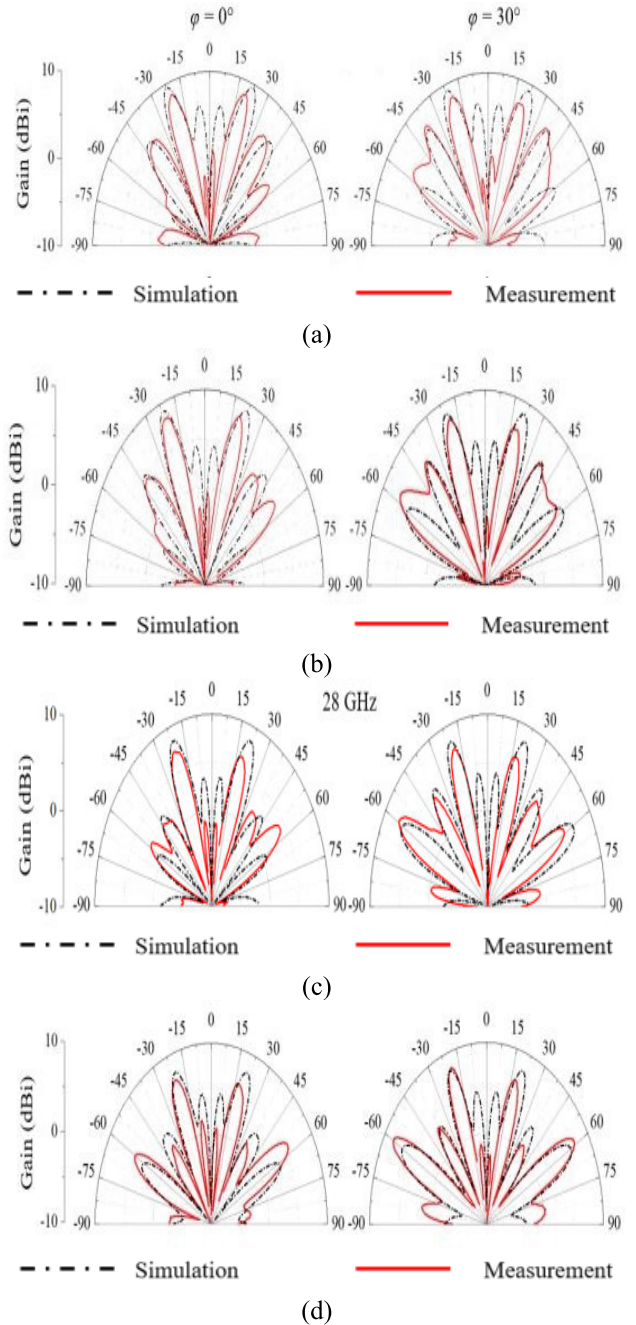
the ground base of the SMA jack to the antenna ground and the center pin of the SMA jack is soldered onto the top driven patch.

A dual band Vivaldi antenna was developed with the intention of functioning at frequencies of 2.4 GHz and 5.8 GHz, both of which are typical frequencies utilized by the radio controllers of drones [37]. The suggested Vivaldi antenna (Fig. 26) is based on a small rectangular region that tapers off into exponential curves at both ends and is activated by a feeding line on the back of the board. Standard drone
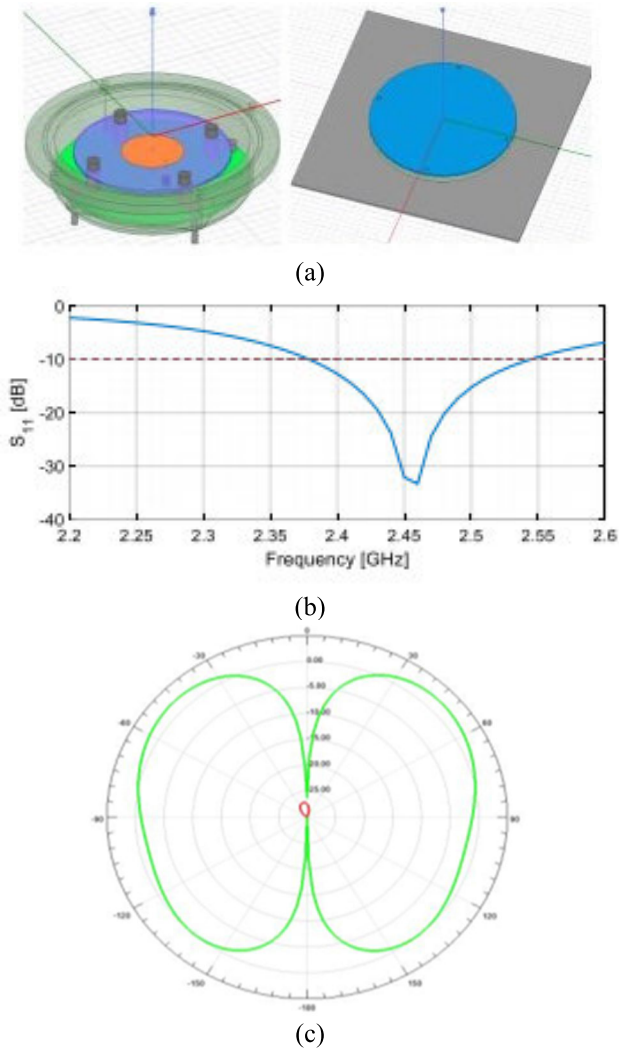
(a)

(b)

(c)

FIGURE 19. The annual ring antenna design, with (a, b) an exposed interior showing the isola IS680-280 substrate in violet and the FR-4 substrate in green, and an AR microstrip antenna embedded in a metallic plate representing an aero plane and protected by a polyethylene (PE) cover & simulated S_{11} of the AR antenna and (c) radiation pattern at 2.4 GHz [34].

(a)

(b)

(c)

FIGURE 20. The prototype of (a) RPA antenna, (b) S11 and (c) Directional antenna radiation pattern for a quadrotor [15].

frequencies are 2.4 GHz and 5.8 GHz (Fig. 27a), and the spacing between the ends of the exponential curves is half the length of the 2.4 GHz wave for operation at these frequencies (62.46 mm). The frequency margin below –10 dB (S_{11}) demonstrated by this antenna was likewise quite impressive. This Vivaldi antenna shown in Fig. 27 (b, c) is a directional antenna because it exhibits particularly high gains in its primary direction. The highest gain of 7.45 dBi (at 5.8 GHz) was achieved by the simulated antenna in this research.

An Unmanned Aerial Vehicle (UAV) and ground station using a dual-band, high-gain communication link where the two bands can be utilized separately for data and command-and-control. High gain is achieved in both frequency ranges by using a proposed cylindrically conformal rectangular patch antenna operating in the higher order TM$_{21}$ and TM$_{03}$ modes [38]. The rectangular patch antenna with the slot
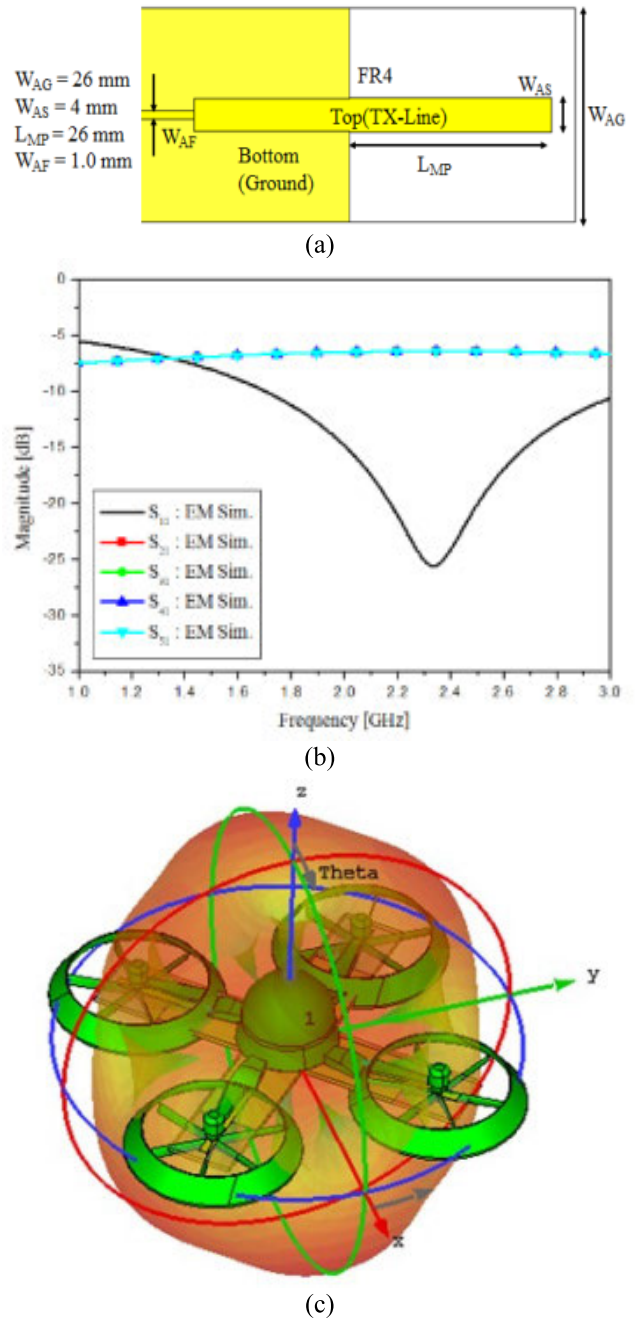
loading is shaped into a cylinder with a 25 mm radius. On a Rogers 5880 substrate with a thickness of 0.508 mm and a loss tangent of 0.0009, a rectangular patch is created with the following dimensions: the length & width of patch, slot, L=20 mm, W=20 mm, Ls=13 mm, Ws=3.5 mm and feed p=8mm. For this aim, a method known as standard lithography is utilized. After that, the patch antenna is shaped to fit inside a cylinder made of Teflon, with a diameter of 25 mm and a height of 7 mm. Fig. 28 (a) illustrates the completed antenna design and construction and Fig. 28 (b) depicts the
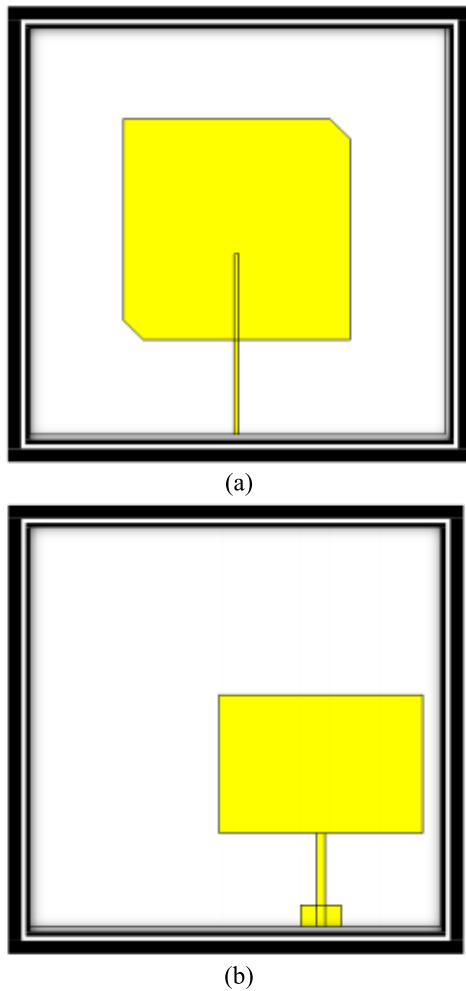
(a)

(b)

FIGURE 21. Dual band combo antenna's (a) top & (b) bottom view [35].

(a)

(b)

FIGURE 22. S_{11} of dual band combo antenna's (a) at 1.575 GHz & (b) 2.45 GHz [35].

antenna's return loss performance. Both the first frequency and the second frequency have been simulated using bandwidths of 192 MHz and 376 MHz respectively. Both the first frequency and the second frequency have been measured to have bandwidths of 213 MHz and 330 MHz.

A 4 × 8 phased array antenna is shown here, along with its design process [39]. First, an electromagnetic energy-coupling unit element in a multilayer architecture with orthogonal slots in the ground plane is created and the physical dimension shown in Fig. 29 (a). The bandwidth is increased to 600 MHz (Fig. 29b) by stacking a patch with truncated edges on the top of a thick substrate layer. Then, a 1 × 4 and 4 × 8 slot connected stacked patch array is designed using this multilayered stacked patch unit element. In order to achieve the desired circular polarization at the antenna feed, a novel feedline structure has been developed for the bottom side. The feedline structure uses a difference in length equal to a quarter wavelength ($\lambda_g/4$) to provide the required phase difference. After the models have been verified numerically, they are physically verified by fabricating 1 × 4 and 4 × 8 stacked patch antenna arrays.

After the models have been verified numerically, they are physically verified by fabricating 1 × 4 and 4 × 8 stacked patch antenna arrays. Overa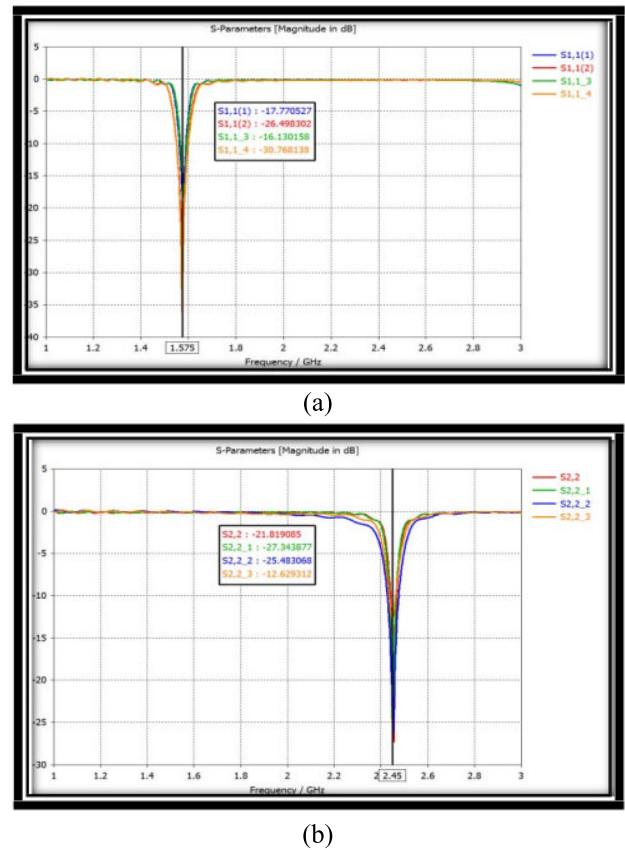ll, the measured and predicted findings demonstrated high agreement, making the suggested constructed array capable of supplying 600 MHz a great option for radar communication, small commercial drones, and synthetic aperture radar. In addition, it is demonstrated that the proposed construction has adequate scanning characteristics up to $\pm$**45°**. In order to improve the proposed PAA's scanning performance at 45° and –45° in the XZ-plane, phase shifters are used to apply the correct phases at the input of the power divider. Fig. 29 (c, d) shows that at the frequency scan losses increase by more than 5 dB from bore sight, even though they remain within this range at $\pm$**45°**. Scanning performance was excellent throughout a range of 90° from 2.4 to 3.0 GHz with the proposed 4 × 8 SAA.

UAVs are increasingly being contemplated for use in situations that require real-time command and control in addition to high bandwidth and low latency communications for the transfer of video and sensor data. This work [40] investigates the design of an antenna and codebook for use in UAV communication at frequencies of 28 GHz and 140 GHz, using antenna simulations and flight patterns that are as realistic as possible. In the scenario involving 28 GHz it has been considered a single circularly polarized patch antenna element
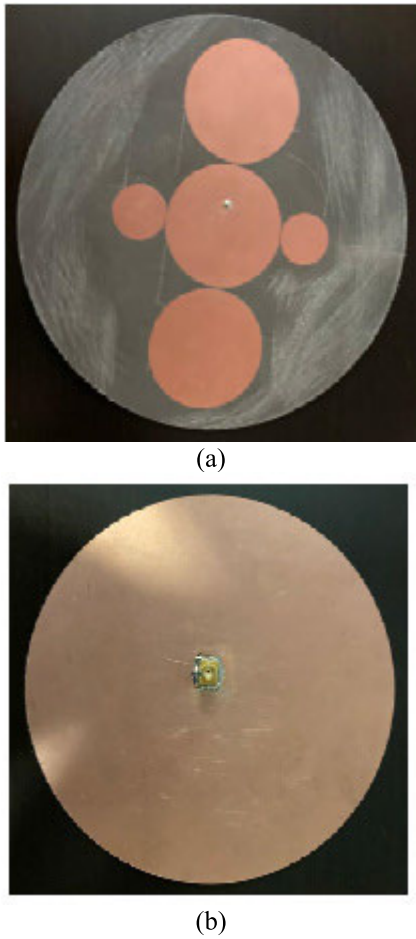
(a)

(b)

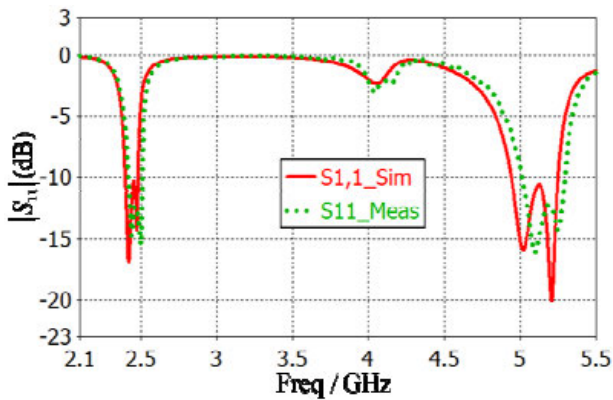**FIGURE 23.** Fabricated of circular patch antenna's (a) front & (b) back side view [36].

FIGURE 24. The comparison of simulated and measured S_{11} of circular patch antenna [36].

(a)

(b)

FIGURE 25. Measure 3-D radiation pattern at (a) 2.4 GHz and (b) 5.2 GHz [36].
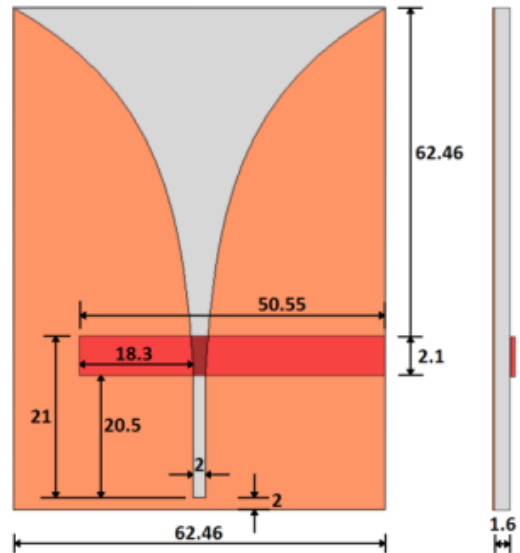
FIGURE 26. Antenna dimensions from both the front (on the left) & the side (right) [37].

mounted on a low-loss Preperm255 substrate. In order to achieve optimal performance at 28 GHz, the feeding point of the patch antenna is shifted away from the center by 1.05 mm, and the antenna itself features a patch antenna element with two opposite corners truncated to enable circular polarization (CP). At 140 GHz, a similar antenna architecture is explored.
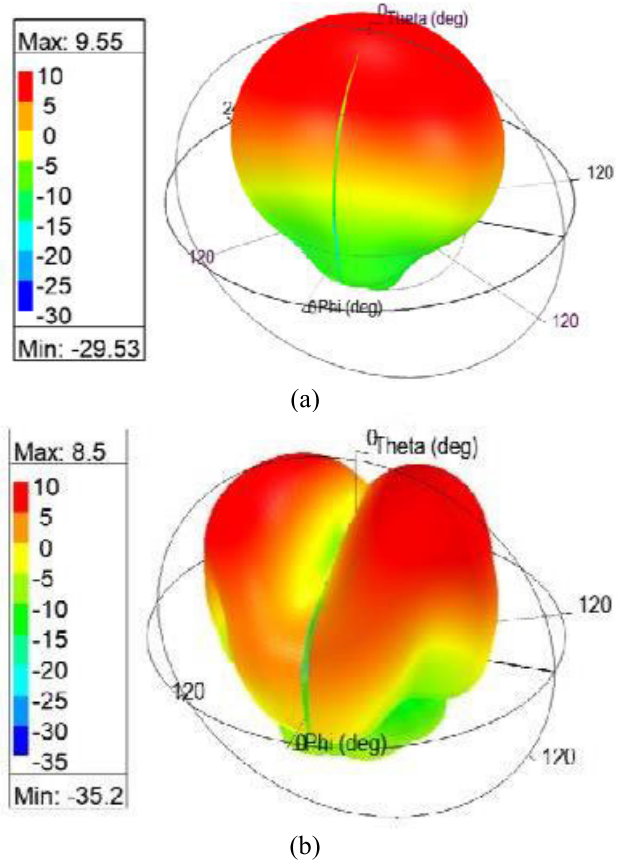
The antenna is planned out on a three-layer Megtron7 substrate and it has been illustrated in Fig. 30 (a) and Fig. 30 (b) shows S_{11} of the designed antenna elements. Evaluate the
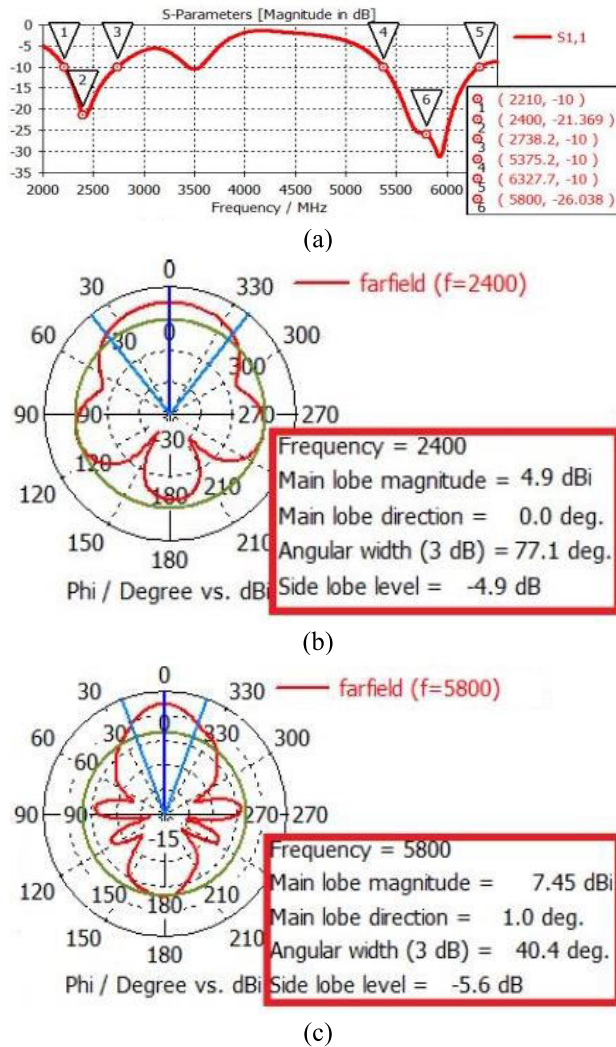
FIGURE 27. The suggested vivaldi antenna's (a) S$_{11}$, 2-D radiation pattern at (b) 2.4 GHz & (c) 5.8 GHz [37].

FIGURE 28. Cylindrically conformal rectangular patch antenna's (a) fabrication picture & (b) return loss [38].

variations in 2–D radiation patterns shown in Fig. 31 (dash black line - antenna in the free space and solid red line - antenna on the drone).

The authors present a unique reconfigurable microstrip magnetic dipole antenna [1] for use in aerial drones, with switchable conical beams. The proposed antenna has three individual cavities that are partitioned by two sets of shorting posts. Multiple p-i-n diodes, wired to the shorting posts, function as RF switches to reorganize the resonant cavities. The antenna has the capability of working in three distinct resonance modes. Fig. 32(a) depicts the outline of the planned antenna. The antenna has a thickness of 1 mm, a relative dielectric constant of 4.4 and a separation of 4.8 mm between two FR4 substrates. A cavity is formed between two metal patches on opposite sides of two substrates which are connected by shorting sidewalls. There are six 1 mm diameter shortening posts labelled a1, a2, a3, b1, b2, and b3. These terminals are coupled to two DC biasing lines, one with voltage
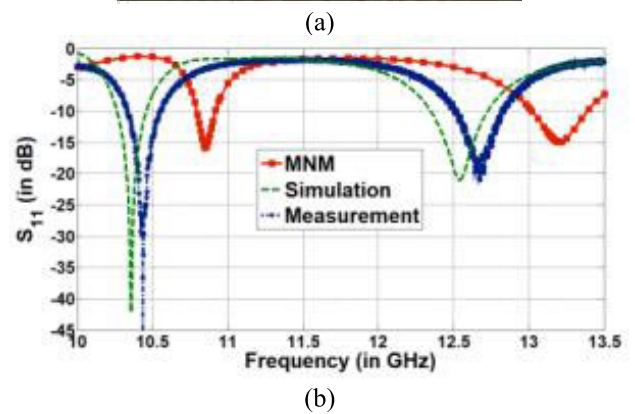
DC#1 and the other with voltage DC#2. Prototype construction is depicted in Fig. 32(b). When the antenna is in its initial operational mode, its resonance frequency is 2.46 GHz. Two resonant frequencies 2.12 GHz and 2.42 GHz are seen for State II, and they are obtained via the TM$^x_{11}$ and TM$^x_{12}$ modes. Three resonant frequencies, at 1.90 GHz, 2.24 GHz, and 2.44 GHz, are found in State III. The WLAN 2.4 GHz application spectrum falls inside the overlap in bandwidth between the three states, which is between 2.39 GHz and 2.49 GHz, illustrated in Fig. 32(c). As can be seen in Fig. 33 (a), the down-tilted conical beam has an elevation angle of 66° and generates a 360° radiation pattern in the azimuth plane for $\theta = 114°$. In Fig. 33 (a, b) the already-inclined conical beams are further angled away from the XY Plane ($\theta = 90°$). It's clear that there's a big difference between the up- and down-tilted beams. It's clear that there's a distinction between the vertically and horizontally slanted beams. With an elevation angle of 54°, the down-tilted conical beam produces a 360° pattern in the azimuth plane at a depth of $\theta = 126°$. All of the antenna's operational modes include a cross-polarization level lower than −13 dB, and the antenna itself is horizontally polarized.
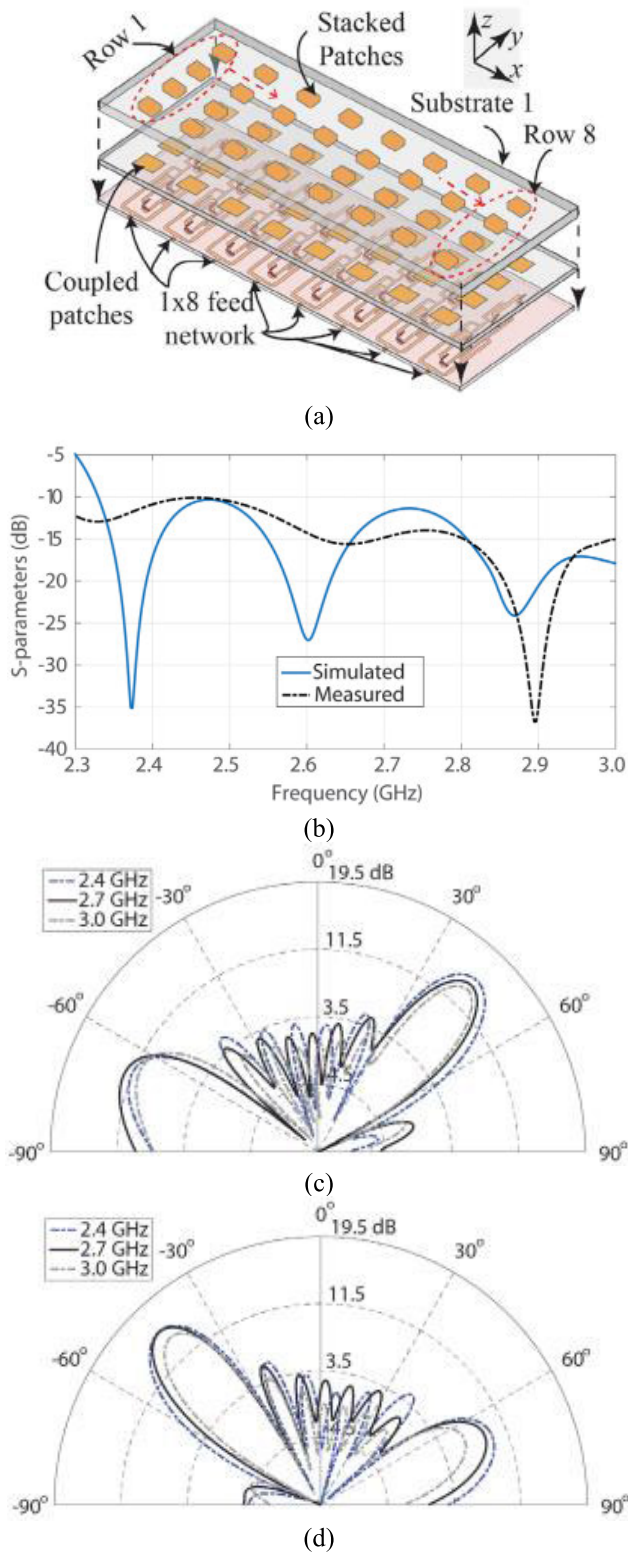
(a)

(b)

(c)

(d)

FIGURE 29. (a) This diagram shows the components of a 4 × 8 phased array with a slot linked patch antenna and (b) measure & simulated S_{11}, antenna array's radiation pattern in the XZ-Plane (azimuth) at 2.4, 2.7, and 3.0 GHz when scanning (c) 45°, (d) −45° of bore sight [39].

A method is proposed for leveraging inkjet printing technology to include antennas into disposable paper drones [41].

(a)

(b)

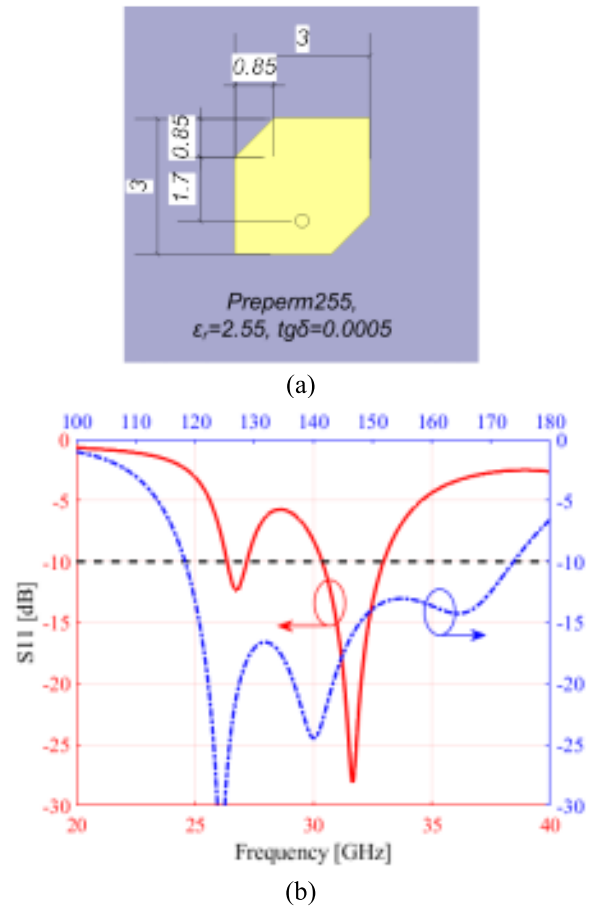**FIGURE 30.** (a) Physical prototype of CP antenna & (b) simulated S_{11} of CP antenna [40].

(a)

(b)

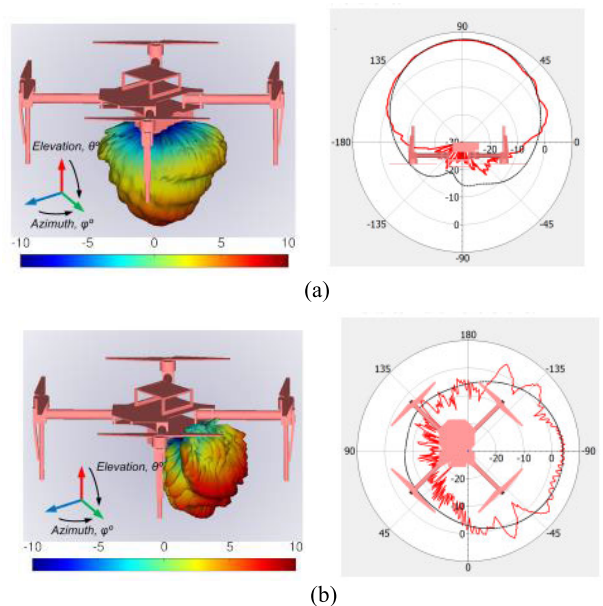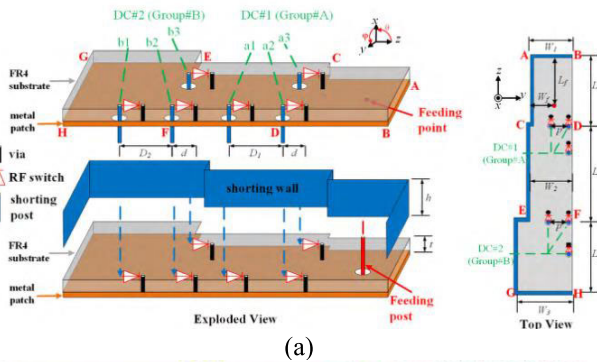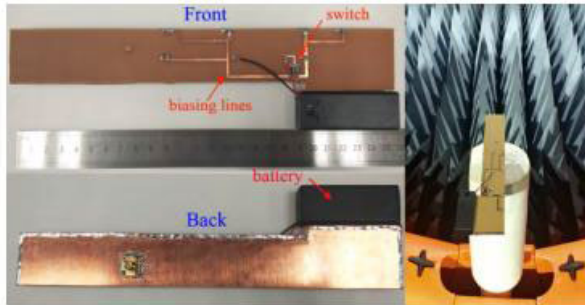**FIGURE 31.** 2-D radiation patterns on a commercial drone reported to be 28 GHz, (a) $\varphi = 0°$ and (b) $\theta = 135°$ [40].
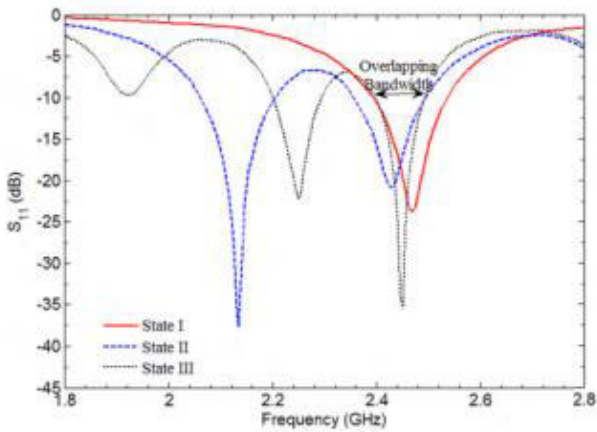
These UAVs or unmanned aerial vehicles are created with the use of origami-based folding structures. The effectiveness of
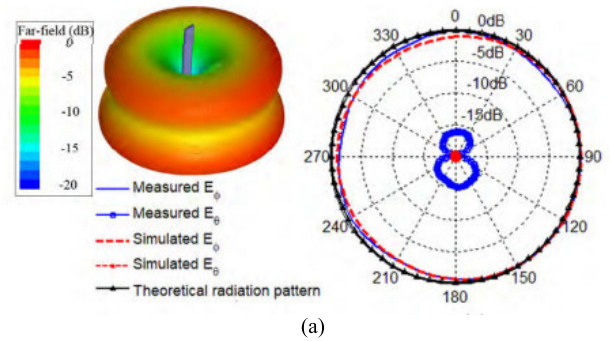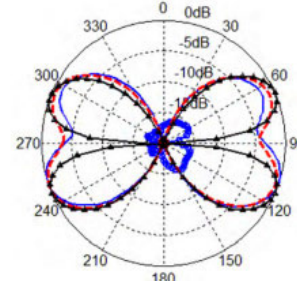
(a)

(b)

(c)

FIGURE 32. (a, b) Photography of the magnetic dipole antenna & **(c)** reflection coefficient measurements made with the proposed antenna in its various operational modes [1].

(a)

(b)

(c)

FIGURE 33. 2–D radiation pattern at 2.44 GHz, (a) azimuth plane for $\theta = 126°$. (b) XZ-Plane and (c) YZ-Plane [1].

the two suggested vertical monopole antennas is compared and contrasted under two distinct scenarios. As shown in Fig. 34(a) the most suitable type of monopole for this purpose is one that has its polarization aligned vertically. In this illustration, the wings have been rendered see-through so that the antenna may be seen. Either a 50Ω transmission line or a specialized matching network can be used to connect the antenna to the other radio frequency (RF) components found in the wings. The frequency ranges of (2.4–2.5) GHz and (5.15–5.9) GHz are the ones that are being targeted. The

initial concept for an antenna that was able to meet these requirements (shown in Fig. 34a) is based on a modified semi-circle that has been given a rectangular shape and a resonant element has been placed to the very top. Since the higher band requires a wide bandwidth, which is matched by the semicircle (L1), the lower band is provided by the inclusion of a T-shaped element with a matching gap (L3), which does not greatly increase the antenna's physical dimensions. Fig. 34(c) displays both the simulated and measured values of the S_{11} parameter and Fig. 34(b) illustrated the testing environment of proposed antenna. There was a small shift to the right in the measured resonant frequencies. Thus, the summary of this section has been illustrated in Table 1. This summary table shows the antennas design techniques with substrate and operating frequencies.

TABLE 1. An overview of different antennas used for drone communication.

| Ref	Antenna design	Size (W×L) (mm²)	Substrate	h (mm)	ε_r	Frequency (GHz)	Gain (dBi)
[1]	Magnetic dipole antenna	102×33.8	FR4	1	4.4	2.39–2.49	4.3
[15]	RPA patch antenna with partial ground	26×26	FR4	1	4.3	2.4	---
[23]	Circularly polarized array	D=7 cm	RO4360G2	1.524	6.15	2.4	---
[24]	CPW antenna with flexible cable	196×15	FR4	0.8	4.4	902–928 MHz	4.5 ± 0.1
[25]	Conformal patch with DGS ground antenna	79.3×72.1	RT Duroid 5880	0.787	2.2	5.05–5.45	10
[26]	4×4 element patch phased array	---	Rogers TM4	---	4.5	5.8	---
[27]	1×4 array antenna	$0.88\lambda_0 \times 0.88\lambda_0$	Taconic TLX-9	1.1	2.5	5.9	7.4
[28]	Conformal partial ground UWB antenna	29×39	Rogers 5880 LZ	1.27	1.97	2.9–15.9	---
[29]	Circular array	D=90, H=50	---	---	2	2.45	---
[30]	Planar quasi-isotropic	85×90	FR4	1.6	---	2–2.4	---
[31]	Rectangular patch	44.06×38	FR4	1.6	4.3	2.4	4
[32]	Planer array antenna with inverted-F antennas	150×200	FR4	0.8	4.4	1.09	3.7
[33]	Conical-beam planer antenna	48×48	Rogers 5880, 5870	1.57,3.18	2.2, 2.33	26.50–29.96	8.51
[34]	Annular ring patch antenna	173.75×173.75	FR4	1	---	2.4	---
[35]	Dual band combo antenna	---	---	---	---	1.575, 2.45	5.08, 6.35
[36]	Dual mode dual band	radius= 76mm	Rogers 5880	1.57	2.2	2.4,5.2	---
[37]	Dual band Vivaldi antenna	62.46×87.06	---	1.6	---	2.4, 5.8	4.9, 7.45
[38]	Cylindrical rectangular patch antenna	$82.4\lambda_0 \times 30\lambda_0$	Rogers 5880	0.508	2.2	10.323,12.46	7.46, 9.83
[39]	4×8 phased array antenna	55×215	Rogers 5880	1.574	2.2	2.4–3	19.5
[40]	CP patch antenna	---	Preperm255, Megtrom7	0.5	2.55, 3.4	28, 140	---
[41]	Flexible two vertical monopole antenna	35.4×30.8	Photo paper	0.18	---	2.4, 5.2, 5.8	---

(a)

(b)

(c)
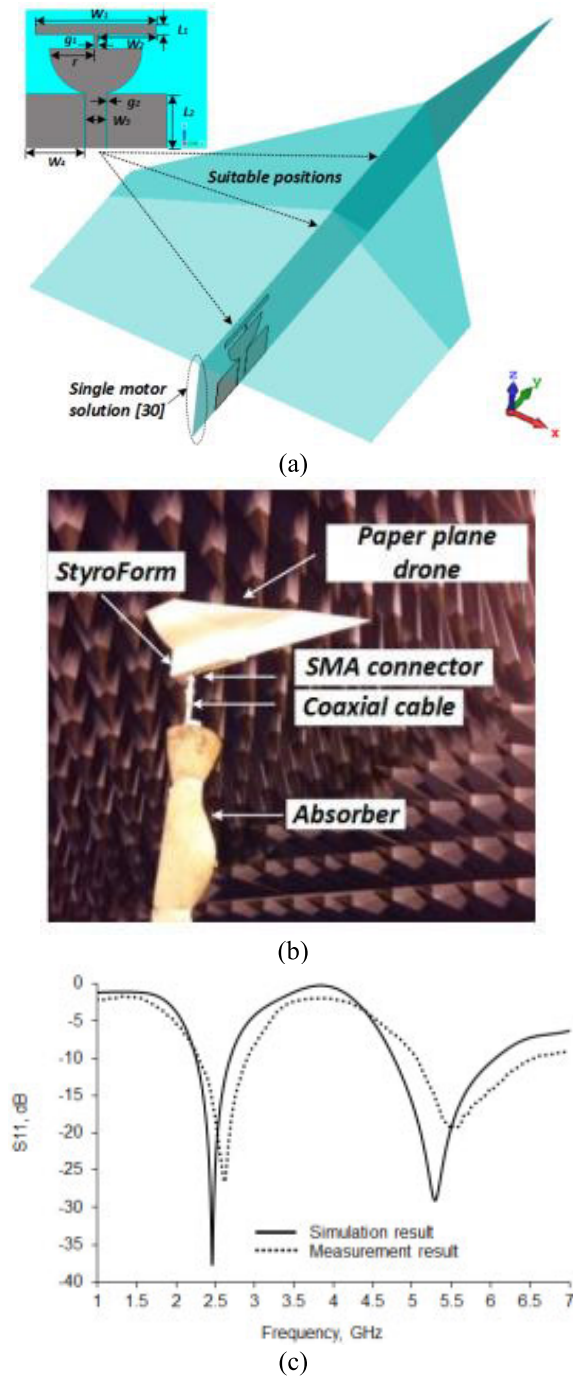
FIGURE 34. (a) Antenna measurements and possible places on an origami drone with a large iron ground plane covering the wings, (b) measurement environment and (c) combination of measured & simulated S$_{11}$ [41].

III. CONCLUSION

Unmanned Aerial Vehicles or UAVs, are also referred to as autonomous drones and they are being used for a variety of purposes including disaster management, search and rescue operations, surveillance, and remote monitoring. In these kinds of situations, the wireless connection that allows the data to be sent from the drone to the ground station or to

another drone is absolutely necessary. Since antennas are the most crucial component of the drone's wireless connection, they need to be built in such a way that they don't get in the way of the drone's movement in the air. In other words, the antenna needs to be small, light, flexible and able to cover a large area. It has been shown that certain types of patch antennas can work for wireless drone communications. For drone communications a vertically polarized omnidirectional antenna is typically the best option. In addition, the entire ground plane mitigates the body effect, making the design attractive as a universal plug-and-play option that is unaffected by the dielectric or metallic composition of the UAV's chassis.

REFERENCES

[1] Z. Liang, Z. Liang, Y. Li, J. Liu, J. Qin, and Y. Long, "Reconfigurable microstrip magnetic dipole antenna with switchable conical beams for aerial drone applications," *IEEE Access*, vol. 7, pp. 31043–31054, 2019.

[2] M. Hassanalian and A. Abdelkefi, "Classifications, applications, and design challenges of drones: A review," *Prog. Aerosp. Sci.*, vol. 91, pp. 99–131, May 2017.

[3] D. R. Viloria, E. L. Solano-Charris, A. Muñoz-Villamizar, and J. R. Montoya-Torres, "Unmanned aerial vehicles/drones in vehicle routing problems: A literature review," *Int. Trans. Oper. Res.*, vol. 28, no. 4, pp. 1626–1657, Jul. 2021.

[4] A. Coluccia, G. Parisi, and A. Fascista, "Detection and classification of multirotor drones in radar sensor networks: A review," *Sensors*, vol. 20, no. 15, p. 4172, Jul. 2020.

[5] N. M. Noor, A. Abdullah, and M. Hashim, "Remote sensing UAV/drones and its applications for urban areas: A review," *IOP Conf. Ser., Earth Environ. Sci.*, vol. 169, Jul. 2018, Art. no. 012003.

[6] D. Floreano and R. J. Wood, "Science, technology and the future of small autonomous drones," *Nature*, vol. 521, no. 7553, pp. 460–466, May 2015.

[7] R. Alyassi, M. Khonji, A. Karapetyan, S. C. Chau, K. Elbassioni, and C. Tseng, "Autonomous recharging and flight mission planning for battery-operated autonomous drones," *IEEE Trans. Autom. Sci. Eng.*, vol. 20, no. 2, pp. 1034–1046, Apr. 2023.

[8] X. Li, H. Huang, and A. V. Savkin, "A novel method for protecting swimmers and surfers from shark attacks using communicating autonomous drones," *IEEE Internet Things J.*, vol. 7, no. 10, pp. 9884–9894, Oct. 2020.

[9] A. Rejeb, K. Rejeb, S. Simske, and H. Treiblmaier, "Humanitarian drones: A review and research agenda," *Internet Things*, vol. 16, Dec. 2021, Art. no. 100434.

[10] A. Nayyar, B.-L. Nguyen, and N. G. Nguyen, "The Internet of Drone Things (IoDT): Future envision of smart drones," in *Proc. 1st Int. Conf. Sustain. Technol. Comput. Intell.*, in Advances in Intelligent Systems and Computing, A. K. Luhach, J. A. Kosa, R. C. Poonia, X.-Z. Gao, and D. Singh, Eds. Singapore: Springer, 2020, pp. 563–580.

[11] J. Xie, J. Yu, J. Wu, Z. Shi, and J. Chen, "Adaptive switching spatial-temporal fusion detection for remote flying drones," *IEEE Trans. Veh. Technol.*, vol. 69, no. 7, pp. 6964–6976, Jul. 2020.

[12] T. Elijah, R. S. Jamisola, Z. Tjiparuro, and M. Namoshe, "A review on control and maneuvering of cooperative fixed-wing drones," *Int. J. Dyn. Control*, vol. 9, no. 3, pp. 1332–1349, Sep. 2021.

[13] W. Saad, M. Bennis, M. Mozaffari, and X. Lin, *Wireless Communications and Networking for Unmanned Aerial Vehicles*. Cambridge, U.K.: Cambridge Univ. Press, 2020.

[14] R. Miura, T. Kagawa, F. Ono, L. Shan, T. Matsuda, and F. Kojima, "Propagation measurements of multi-hop command and telemetry communications system in the 169 MHz band for drones," *J. Robot. Mechatronics*, vol. 33, no. 2, pp. 363–370, Apr. 2021.

[15] Y. Seo, M. Jeon, J. Cho, Y. Lee, J. Jang, C. Lee, and S. Kahng, "A small and angle-diversity antenna mountable for the small drone," in *Proc. Int. Conf. Inf. Commun. Technol. Converg. (ICTC)*, Oct. 2021, pp. 994–996.

[16] S. Kim and J. Choi, "Beam steering antenna with reconfigurable parasitic elements for FPV drone applications," *Microw. Opt. Technol. Lett.*, vol. 60, no. 9, pp. 2173–2177, Sep. 2018.

[17] A. Bansal and R. Gupta, "A review on microstrip patch antenna and feeding techniques," *Int. J. Inf. Technol.*, vol. 12, no. 1, pp. 149–154, Mar. 2020.

[18] V. Prakasam, K. R. A. LaxmiKanth, and P. Srinivasu, "Design and simulation of circular microstrip patch antenna with line feed wireless communication application," in *Proc. 4th Int. Conf. Intell. Comput. Control Syst. (ICICCS)*, May 2020, pp. 279–284.

[19] M. U. Khan, M. S. Sharawi, and R. Mittra, "Microstrip patch antenna miniaturisation techniques: A review," *IET Microw., Antennas Propag.*, vol. 9, no. 9, pp. 913–922, Jun. 2015.

[20] A. Salari and D. Erricolo, "Unmanned aerial vehicles for high-frequency measurements: An accurate, fast, and cost-effective technology," *IEEE Antennas Propag. Mag.*, vol. 64, no. 1, pp. 39–49, Feb. 2022.

[21] M. Longhi and G. Marrocco, "Ubiquitous flying sensor antennas: Radiofrequency identification meets micro drones," *IEEE J. Radio Freq. Identificat.*, vol. 1, no. 4, pp. 291–299, Dec. 2017.

[22] C. Schovaers, C. Craeye, and F. Glineur, "Calibration of SKA-low antenna array using drones," Ecole Polytechn. de Louvain, Université Catholique de Louvain, Ottignies-Louvain-la-Neuve, Belgium, 2019.

[23] V. Araña-Pulido, E. Jiménez-Yguácel, F. Cabrera-Almeida, and P. Quintana-Morales, "Antenna system for trilateral drone precise vertical landing," *IEEE Trans. Instrum. Meas.*, vol. 71, pp. 1–8, 2022.

[24] X. Yang, Y. Qi, B. Yuan, Y. Cao, and G. Wang, "A miniaturized high-gain flexible antenna for UAV applications," *Int. J. Antennas Propag.*, vol. 2021, Jul. 2021, Art. no. e9919425.

[25] J. Monica and P. Jothilakshmi, "Gain enhanced conformal patch antenna with defected ground for aircraft applications," *IET Commun.*, vol. 14, no. 2, pp. 290–299, Jan. 2020.

[26] J. Shearwood, N. Aldabashi, A. Eltokhy, E. L. Franklin, N. E. Raine, C. Zhang, E. Palmer, P. Cross, and C. Palego, "C-band telemetry of insect pollinators using a miniature transmitter and a self-piloted drone," *IEEE Trans. Microw. Theory Techn.*, vol. 69, no. 1, pp. 938–946, Jan. 2021.

[27] C. U. Lee, G. Noh, B. Ahn, J.-W. Yu, and H. L. Lee, "Tilted-beam switched array antenna for UAV mounted radar applications with 360° coverage," *Electronics*, vol. 8, no. 11, p. 1240, Oct. 2019.

[28] L. I. Balderas, A. Reyna, M. A. Panduro, C. D. Rio, and A. R. Gutiérrez, "Low-profile conformal UWB antenna for UAV applications," *IEEE Access*, vol. 7, pp. 127486–127494, 2019.

[29] D. V. Navarro-Méndez, H. C. Moy-Li, L. F. Carrrera-Suárez, M. Ferrando-Bataller, and M. Baquero-Escudero, "Antenna arrays for unmanned aerial vehicle," in *Proc. 9th Eur. Conf. Antennas Propag. (EuCAP)*, Apr. 2015, pp. 1–5.

[30] S. I. H. Shah, M. M. Tentzeris, and S. Lim, "Planar quasi-isotropic antenna for drone communication," *Microw. Opt. Technol. Lett.*, vol. 60, no. 5, pp. 1290–1295, May 2018.

[31] A. Reyna, J. C. Garza, O. Elizarraras, M. Panduro, L. I. Balderas, and M. D. L. L. Prado, "3D random virtual antenna arrays for FANETs wireless links," *Telecommun. Syst.*, vol. 77, no. 3, pp. 469–477, Jul. 2021.

[32] A. Sidibe, G. Loubet, A. Takacs, G. Ferré, and A. Ghiotto, "Miniature drone antenna design for the detection of airliners," *Int. J. Microw. Wireless Technol.*, vol. 13, no. 1, pp. 21–27, Feb. 2021.

[33] D. A. Pham, M. Lee, and S. Lim, "High-gain conical-beam planar antenna for millimeter-wave drone applications," *IEEE Trans. Antennas Propag.*, vol. 69, no. 10, pp. 6959–6964, Oct. 2021.

[34] E. Giampietri, F. Molesti, G. Nenna, and A. Monorchio, "A compact annular ring microstrip antenna for unmanned aerial vehicles (UAVs) applications," in *Proc. IEEE Int. Symp. Antennas Propag. USNC-URSI Radio Sci. Meeting (APS/URSI)*, Dec. 2021, pp. 1962–1963.

[35] M. A. Jamlos, W. A. Mustafa, S. Z. S. Idrus, and N. Fatin, "Dual-band frequency antenna for drone application," *J. Phys., Conf. Ser.*, vol. 1529, no. 2, Apr. 2020, Art. no. 022083.

[36] Z. Akhter, R. M. Bilal, and A. Shamim, "Dual-mode circular microstrip patch antenna for airborne applications," in *Proc. 15th Eur. Conf. Antennas Propag. (EuCAP)*, Mar. 2021, pp. 1–5.

[37] L. Astini, L. Manera, and M. Donatti, "Dual band Vivaldi antenna design and electromagnetic simulation for drone spoofing," in *Proc. XXV Congresso de Iniciação Científica da UNICAMP*, 2017.

[38] S. Pradhan and B. Gupta, "High-gain dual-mode cylindrical rectangular patch antenna for airborne applications," *IEEE Trans. Aerosp. Electron. Syst.*, vol. 58, no. 5, pp. 4168–4179, Oct. 2022.

[39] M. S. Khan, A. Iftikhar, S. A. Naqvi, B. Ijaz, A. Fida, R. M. Shubair, and S. A. Khan, "Circularly polarized 4 × 8 stacked patch antenna phased array with enhanced bandwidth for commercial drones," *Int. J. RF Microw. Comput.-Aided Eng.*, vol. 30, no. 3, Mar. 2020, Art. no. e22081.

[40] W. Xia, V. Semkin, M. Mezzavilla, G. Loianno, and S. Rangan, "Multi-array designs for mmWave and sub-THz communication to UAVs," in *Proc. IEEE 21st Int. Workshop Signal Process. Adv. Wireless Commun. (SPAWC)*, Atlanta, GA, USA, May 2020, pp. 1–5.

[41] S. Y. Jun, A. Shastri, B. Sanz-Izquierdo, D. Bird, and A. McClelland, "Investigation of antennas integrated into disposable unmanned aerial vehicles," *IEEE Trans. Veh. Technol.*, vol. 68, no. 1, pp. 604–612, Jan. 2019.

M. M. HASAN MAHFUZ (Graduate Student Member, IEEE) was born in Gazipur, Dhaka, Bangladesh, in 1993. He received the B.Sc. and M.Sc. degrees in electrical and computer engineering. He is currently pursuing the Ph.D. degree with the University of Quebec at Rimouski, Canada. His current research interests include microstrip patch antennas, wearable textile antennas for biomedical applications, array antennas, automotive radar systems, head imagine systems, and the applications of the phased array antennas.

CHAN-WANG PARK (Member, IEEE) received the B.Sc. degree in electronic and communication engineering from Han Yang University, Seoul, South Korea, in 1981, the M.Sc. degree from ENST de Paris, France, in 1996, and the Ph.D. degree from IEMN, Université des Sciences et Technologies de Lille 1, France, in 2001. From 1981 to 1985, he was with the Research and Development Center, Gold Star Electric (LG Telecom), Anyang, South Korea. From 1985 to 1990, he was with the Training Centre, Saudi Telecom, as a Technical Instructor. From 1990 to 1994, he developed three satellites with the Satellite Technology Research Centre, KAIST, South Korea, as a Project Manager. From 1994 to 1995, he was with IAS and Matra Marconi Space, France. From 2001 to 2002, he was with AmpliX and Mitec Telecom, Canada. In 2003, he joined Université du Québec à Rimouski, where he is currently a Professor. His research interests include antenna design, high power amplifier design, the characterization of transistor, and RF/microwave and millimeter wave components design.

• • •